eNeuro

*Research Article: New Research | Cognition and Behavior*

# Reduced Vglut2/Slc17a6 gene expression levels throughout the mouse subthalamic nucleus cause cell loss and structural disorganization followed by increased motor activity and decreased sugar consumption

STN Vglut2 reduction perturbs movement and reward

**Nadine Schweizer[1,*], Thomas Vierecklel[1,2,*], Casey J. A. Smith-Anttila[2], Karin Nordenankar[2], Emma Arvidsson[1], Souha Mahmoudi[3], André Zampera[6], Hanna Wärner Jonsson[4], Jonas Bergquist[5], Daniel Lévesque[3], Åsa Konradsson-Geuken[1], Malin Andersson[4], Sylvie Dumas[6] and Åsa Wallén-Mackenzie[1]**

[1]*Department of Organismal Biology, Uppsala University, SE-752 36 Uppsala, Sweden*
[2]*Department of Neuroscience, Uppsala University, SE-751 24 Uppsala, Sweden*
[3]*Faculty of Pharmacy, Université de Montréal, Montréal, QC H3T 1J4, Canada*
[4]*Department of Pharmaceutical Biosciences, Uppsala University, SE-751 24 Uppsala, Sweden*
[5]*Department of Chemistry, BMC - Analytical Chemistry and Neurochemistry, Uppsala University, SE-751 24 Uppsala, Sweden*
[6]*Oramacell, 75006 Paris, France*

DOI: 10.1523/ENEURO.0264-16.2016

Received: 2 September 2016

Accepted: 8 September 2016

Published: 15 September 2016

**Author contributions:** N.S., T.V., C.J.S.-A., D.L., x.K.-G., M.A., S.D., and x.W.-M. designed research; N.S., T.V., C.J.S.-A., K.N., E.A., S.M., A.Z., H.W.J., J.B., D.L., M.A., S.D., and x.W.-M. performed research; N.S., T.V., C.J.S.-A., A.Z., J.B., D.L., x.K.-G., M.A., S.D., and x.W.-M. analyzed data; N.S., T.V., C.J.S.-A., x.K.-G., and x.W.-M. wrote the paper.

**Funding:** Swedish research council: 2013-4657; 2014-3804; 2011-4423; 2015-4870; 2012-2304. The brain foundation; Bertil Hållsten Research Foundation; Foundation of Gösta Lind; Foundation of Åhlén; Foundation of Åke Wiberg;

The authors declare no competing interests. Sylvie Dumas is the owner of Oramacell, Paris, France.

This work was supported by grants from the Swedish Research Council (Vetenskapsrådet 2013-4657, 2014-3804, 2011-4423, 2015-4870, 2012-2304), Uppsala University, the Swedish Brain Foundation, Parkinsonfonden, Bertil Hållsten Research Foundation and the research foundations of Gösta Lind, Åhlén and Åke Wiberg.

*These authors contributed equally to the work

**Correspondence should be addressed to** either Åsa Wallén-Mackenzie, Uppsala University, Department of Organismal Biology/Comparative Physiology, Norbyvägen 18A, SE-752 36 Uppsala, Sweden. Telephone: +46-18-471 6419. E-mail: asa.mackenzie@ebc.uu.se

**Cite as:** eNeuro 2016; 10.1523/ENEURO.0264-16.2016

# Reduced *Vglut2/Slc17a6* gene expression levels throughout the mouse subthalamic nucleus cause cell loss and structural disorganization followed by increased motor activity and decreased sugar consumption

*Abbreviated title: STN Vglut2 reduction perturbs movement and reward*

Nadine Schweizer[1,9*], Thomas Viereckel[1,2*], Casey J.A. Smith-Anttila[2,7], Karin Nordenankar[2,9], Emma Arvidsson[1,8], Souha Mahmoudi[3], André Zampera[6], Hanna Wärner Jonsson[4], Jonas Bergquist[5], Daniel Lévesque[3], Åsa Konradsson-Geuken[1], Malin Andersson[4], Sylvie Dumas[6] and Åsa Wallén-Mackenzie[1#]

[1]Department of Organismal Biology, Uppsala University, SE-752 36 Uppsala, Sweden.

[2]Department of Neuroscience, Uppsala University, SE-751 24 Uppsala, Sweden.

[3]Faculty of Pharmacy, Université de Montréal, Montréal, QC H3T 1J4, Canada.

[4]Department of Pharmaceutical Biosciences, Uppsala University, SE-751 24 Uppsala, Sweden.

[5]Department of Chemistry, BMC - Analytical Chemistry and Neurochemistry, Uppsala University, SE-751 24 Uppsala, Sweden.

[6]Oramacell, 75006 Paris, France.

[7]Current address: Department of Anatomy and Neurosciences, The University of Melbourne, Victoria 3010, Australia.

[8]Current address: Department of Neuroscience, Karolinska Institutet, SE-171 77 Stockholm, Sweden.

[9]Current address: Department of Pharmaceutical Biosciences, Uppsala University, SE-751 24 Uppsala, Sweden.

* These authors contributed equally to the work

# Submitting and Corresponding author: Professor Åsa Wallén-Mackenzie, Uppsala University, Department of Organismal Biology/Comparative Physiology, Norbyvägen 18A, SE-752 36 Uppsala, Sweden. Telephone: +46-18-471 6419. E-mail: asa.mackenzie@ebc.uu.se

Number of pages: 42; Number of figures: 8

Number of words: Abstract: 249, Introduction: 744, Discussion: 1770

## Conflict of interest

The authors declare no competing interests. Sylvie Dumas is the owner of Oramacell, Paris, France.

## Acknowledgements

We thank Ms Anna Andrén for expert technical assistance and the Image platform at Institut de la Vision (Paris, France) for performing image scanning. Prof. James Martin, Baylor College of Medicine (Texas, USA), is thanked for generously sharing *Pitx2-Cre* transgenic mice. We thank all members of the Mackenzie lab for constructive feedback.

This work was supported by grants from the Swedish Research Council (Vetenskapsrådet 2013-4657, 2014-3804, 2011-4423, 2015-4870, 2012-2304), Uppsala University, the Swedish Brain Foundation, Parkinsonfonden, Bertil Hållsten Research Foundation and the research foundations of Gösta Lind, Åhlén and Åke Wiberg.

**Abstract**

The subthalamic nucleus (STN) plays a central role in motor, cognitive and affective behavior. Deep brain stimulation (DBS) of the STN is the most common surgical intervention of advanced Parkinson´s disease (PD) and STN has lately gained attention as target for DBS in neuropsychiatric disorders, including obsessive compulsive disorder, eating disorders and addiction. Animal studies using either STN-DBS, lesioning or inactivation of STN neurons have been used extensively alongside clinical studies to unravel the structural organization, circuitry and function of the STN. Recent studies in rodent STN models have exposed different roles for STN neurons in reward-related functions. We have previously shown that the majority of STN neurons express the *Vesicular glutamate transporter 2* (*Vglut2/Slc17a6*) gene and that reduction of Vglut2 mRNA levels within the STN of mice (cKO) causes reduced post-synaptic activity and behavioral hyperlocomotion. The cKO mice showed less interest in fatty rewards, which motivated analysis of reward-response. The current results demonstrate decreased sugar consumption and strong rearing behavior while biochemical analyses show altered dopaminergic and peptidergic activity in the striatum. The behavioral alterations were in fact correlated with opposite effects in the dorsal versus the ventral striatum. Significant cell loss and disorganization of the STN structure was identified which likely accounts for the observed alterations. Rare genetic variants of the human VGLUT2 gene exist and this study shows that reduced *Vglut2/Slc17a6* gene expression levels exclusively within the STN of mice is sufficient to cause strong modifications in both the STN and in the mesostriatal dopamine system.

## Significance Statement

The STN is the most commonly used target in deep brain stimulation of advanced Parkinson´s disease and it has recently been implicated in the reward circuit. VGLUT2 is the main vesicular transporter of glutamate in STN neurons and rare genetic variants of the VGLUT2 gene exist in human individuals. Blunting *Vglut2/Slc17a6* gene expression levels throughout the extent of the mouse STN caused substantial cell loss in the STN, similar as observed in pharmacological lesion models. Mice became hyperactive but showed reduced sugar consumption. Opposite effects on motor versus reward behavior was correlated with opposite activity of dopamine parameters in the dorsal versus the ventral striatal system. This study thereby identifies an interaction between the STN and the dopamine reinforcement system.

## Introduction

The subthalamic nucleus (STN) is an excitatory structure which via extensive glutamatergic projections plays a central role in motor, limbic and cognitive functions. Dysregulated excitatory output from the STN can be normalized by high frequency deep brain stimulation (DBS). Clinically, STN-DBS is implemented routinely for alleviation of motor dysfunction in in patients suffering from advanced Parkinson's disease (PD) (Benabid et al., 2009), and based on its role in limbic and cognitive functions, the STN has been proposed as a putative target also in DBS approaches to treat various neuropsychiatric disorders (Williams et al., 2010; Chabardès et al., 2013). In fact, STN-DBS has been tested already with positive outcome in severe obsessive compulsive disorder (OCD) (Mallet et al., 2008; Blomstedt et al., 2013).

In parallel to clinical studies of the STN, experimental animals have been used extensively to unravel the structural organization and circuitry of the STN as well as functional outcome upon STN intervention (Temel et al., 2005a; Baunez and Gubellini, 2010). In addition to STN-DBS experiments in animals, other models implement pharmacological lesioning or inactivation to disturb STN function (Temel et al., 2005a; Pratt et al., 2012). Recently, a series of studies in rodent STN models have implicated the STN in the brain reward circuit alongside the classical mesoaccumbal reward pathway (Breysse et al., 2015). First, implementation of STN-DBS and STN-lesioning were shown to elevate the motivation for food while reducing the motivation for cocaine (Baunez et al., 2002, 2005; Bezzina et al., 2008; Rouaud et al., 2010). Second, the presentation of either a positive (rewarding) or negative (aversive) stimulus, or to cues conditioned to either stimulus, altered the firing pattern of neurons within the STN (Darbaky et al., 2005; Lardeux et al., 2009; Espinosa-Parrilla et al., 2013; Breysse et al., 2015). Third, while the question of the structural organization of the STN is the focus of debate between those favoring the hypothesis of the

STN as a tripartite structure and those favoring an STN organization without strict anatomical boundaries (Temel et al., 2005b; Benarroch, 2008; Keuken et al., 2012; Alkemade and Forstmann, 2014), some recent studies have focused on identifying subpopulations of STN neurons. By electrophysiological profiling in rodents, distinct STN subpopulations were found that adapted their responses when the rewarding substance sucrose was exchanged for water (Lardeux et al., 2009, 2013) or an aversive substance, such as quinine (Breysse et al., 2015).

Thus, by adapting to various reward-related contexts, STN neurons form a cerebral hub which participates in even more aspects of motor, limbic and cognitive functions than previously thought. Similar to the etiology of PD, to which aberrant STN activity is believed to contribute (Rodriguez et al., 1998; Olanow and Tatton, 1999), dysfunctional STN activity may therefore contribute to reward dysfunction in patients. Clinically, a putative role in reward-related behavior is manifested by the recent proposals of the STN as a DBS-target for treatment of addiction, eating disorders and obesity (Pelloux and Baunez, 2013; Val-Laillet et al., 2015).

The multitude of roles ascribed to the STN further strengthens the case for solving how this compact nucleus is organized to encompass such a high level of complexity. Based on the excitatory nature of the STN, we recently addressed expression of the genes encoding the three different Vesicular glutamate transporters (VGLUT1-3) in mice (Takamori, 2006; Liguz-Lecznar and Skangiel-Kramska, 2007) and could show that the vast majority of STN neurons express only the *Vglut2/Slc17a6* gene (Schweizer et al., 2014). While a full knockout of the *Vglut2/Slc17a6* gene was previously demonstrated as lethal (Moechars et al., 2006; Wallén-Mackenzie et al., 2006), some rare genetic variants of the human VGLUT2/SLC17A6 gene have been identified in schizophrenia and severe alcoholism (Flatscher-Bader et al., 2008; Shen et al., 2010; Comasco et al., 2014). By implementing conditional targeting of the

*Vglut2/Slc17a6* gene in mice using the *Paired-like homeodomain 2* (*Pitx2*)-*Cre*-driver to direct the targeting to the STN (Skidmore et al., 2008), Vglut2 mRNA levels were reduced by 40% exclusively within the STN structure (Schweizer et al., 2014). This reduction was shown to result in decreased post-synaptic excitatory activity in STN target neurons followed through by strong behavioral hyperactivity, including decreased latency to movement (Schweizer et al., 2014). Despite hyperactivity, these STN-targeted mice did not perform poorer in reward-baited memory and impulsivity tests but did take longer to collect the rewards. This finding led us to here address the hypothesis that the *Pitx2/Vglut2* co-expressing subpopulation of STN neurons is important for regulation of both motor activity and reward-related behavior.

## Materials and Methods

### *Ethical statement*

All mice used in the study were housed and produced as previously described (Schweizer et al., 2014) in accordance with the Swedish regulation guidelines (Animal Welfare Act SFS 1998:56) and European Union legislation (Convention ETS123 and Directive 2010/63/EU). Ethical approval was obtained from the Uppsala Animal Ethical Committee.

The *Vglut2*$^{f/f;Pitx2\text{-}Cre}$ mouse line was produced by breeding *Pitx2-Cre* male mice (Skidmore et al., 2008) to floxed *Vglut2*$^{f/f}$ females (Wallén-Mackenzie et al., 2006) to generate *Vglut2*$^{f/wt;Pitx2\text{-}Cre+}$ male mice which in turn where bred to *Vglut2*$^{f/f}$ females to generate cKO (*Vglut2*$^{f/f;Pitx2\text{-}Cre+}$) and control (*Vglut2*$^{f/f;Pitx2\text{-}Cre-}$) mice. This allows for behavioral phenotyping and comparison between genotype groups due to identical genetic background (Crusio, 2004). Control *Vglut2*$^{wt/wt;Pitx2\text{-}Cre+}$ animals were used in the tracing experiment. All mice were kept on a hybrid background of C57BL/6J and Sv129.

### *Operant self-administration of sucrose*

23 adult mice (13 males, of which cKO, n=7; Ctrl, n=6; 10 females, of which cKO, n=5; Ctrl, n=5) were used to analyze the behavioral response to sugar in an operant self-administration setup (Med Associates, USA) (Skinner, 1966; Sanchis-Segura and Spanagel, 2006). Source data for this experiment, summarized in Figure 2 is available at: http://goo.gl/slIH4u. An outline of the experiment is shown in ***Fig. 2A***, and an illustration of the operant chamber in ***Fig. 2B***. Two days prior and throughout the trial, the mice were under mild food-restriction [3 grams standard rodent chow (R3; Lactamin/Lantmännen, Sweden) per mouse per day] and thereafter weighed throughout the entire course of the experiment. Water was accessible *ad libitum*. The mice were allowed to habituate to the novel environment for 1 session before begin of training and each mouse underwent one operant session per day. The mice were then trained to enter their head into a feeder equipped with a food receptacle and

a photo beam sensor to obtain a 20 mg sucrose pellet (5TUL TestDiet). Each pellet delivery was followed by a 10 s time-out period, in which head entries were registered, but no pellet could be obtained. Training (acquision of the operant task) was performed on a fixed ratio (FR) 1 schedule (1 pellet / head entry, maximum 30 pellets). While a house-light was continuously on, a cue-light was only lit upon head entry into the feeder giving sugar, which also led to the presentation of a sound cue (***Fig. 2B, left***). Head entry into an inactive feeder did not result in cue or sugar presentation (***Fig. 2B, right***). During the timeout period, no cue-light or sound cue was presented. FR1 training was followed by 3 days of testing on FR1 and then on FR5 to assess consummatory behavior. Before advancing the mice to an FR5 schedule (1 pellet / 5 head entries), they were given one training day at FR2 to adjust to a task requiring multiple head entries. The mice were assessed in an FR5 schedule for 5 days, after which motivation to work for the sugar pellets was measured on a progressive ratio (PR) schedule during which the amount of head entries required to obtain a pellet was successively increased by 3 per successful action. After this followed extinction, reinstatement and reversal of active and inactive feeders to assess for task learning and cognitive flexibility.

During all trial days, the mice were left in the self-administration chambers until 30 sugar pellets were obtained (FR1, FR2, reinstatement and reversal) or until trial time ended (FR5, PR and extinction). Trial time was limited to 30 minutes for FR1, FR2, reinstatement, extinction and reversal; to 40 minutes for FR5; to 90 minutes for PR, the maximum time possible for all animals to complete the PR task during the light-cycle of the day. Statistical analysis was performed in GraphPad Prism 6 using repeated measures analysis of variance (ANOVA) and Bonferroni post-hoc test (GraphPad Software, USA). A p-value equal to or less than 0.05 was considered significant (*$p \leq 0.05$, **$p \leq 0.01$, ***$p \leq 0.001$, ****$p \leq 0.0001$).

*Analysis of rearing behavior*

31 adult mice (cKO n=14, Ctrl n=17) were each placed in the center of a square plexiglas arena (55x55x22cm) and allowed to freely explore for 15 minutes. The mice were video-recorded; behavioral parameters were scored manually by an observer blind to the genotype of the mouse and the duration of each rearing type was analyzed using AniTracker Software. Rearing behavior was subdivided into three different types: Wall rearing, defined as an upright position with the fore-paws touching a vertical surface (***Fig. 4A, left***); seated rearing defined by a half-standing position using the tail for support (***Fig. 4B, left***); and free rearing, in which the mouse supports its weight freely on its hind legs without using its tail or fore paws (***Fig. 4C, left***), similar as previously described by (Waddington et al., 2001). Data was analyzed using Mann-Whitney U-test (GraphPad Prism, GraphPad Software, USA). A p-value equal to or less than 0.05 was considered significant (*p≤0.05, **p≤0.01, ***p≤0.001, ****p≤0.0001).

*Dopamine receptors and transporters binding assay*

Brains of cKO and control mice (cKO, n=7; Ctrl, n=7) were rapidly removed from the skull upon cervical dislocation, cryosectioned and processed for DA receptor and transporter autoradiography, as previously described (Mahmoudi et al., 2014; Schweizer et al., 2014). For DA D1 receptor (D1R) binding, the [$^{3}$H]SCH23390 ligand was used. For the DA D2 receptor (D2R) and D3 receptor (D3R) subtypes, [$^{125}$I]iodosulpride and [$^{125}$I]7-OH-PIPAT ligands were used, respectively. [$^{125}$I]RTI-121 binding was used to measure dopamine transporter (DAT) density. Mann-Whitney U-test was performed for statistical analysis. A p-value equal to or less than 0.05 was considered significant (*p≤0.05, **p≤0.01, ***p≤0.001). All values are given as mean ± S.E.M., if not otherwise stated.

*Matrix-assisted laser desorption/ionization imaging mass spectrometry*

Brains of cKO and control mice were cryosectioned at 12 µm and sections encompassing the striatum and GP/EP were thaw-mounted with Pertex (HistoLab Products AB, Sweden) on MALDI imaging compatible conductive glass slides (Bruker Daltonics, Germany). The slides were dried in a vacuum desiccator for 20 minutes and then stored at -20$^{o}$C. Before analysis, the sections were thawed in a desiccator for 30 minutes and then washed 10 seconds in i) 70% ethanol, ii) 95% ethanol, iii) 95% ethanol (Solveco Chemicals AB, Sweden) and iv) 30-seconds in an acid wash (95% ethanol and 5% glacial acetic acid) (Merck, Sweden). The washing steps and matrix deposition has earlier been developed for rat brain sections (Groseclose et al., 2007; Andersson et al., 2008).

Matrix was deposited by a piezoelectric-based Chemical Ink-jet Printer (ChIP-1000, Shimadzu Co, Japan) to apply approximately 100 picoliter-sized drops of matrix in a grid across the tissue sections at a resolution of 200 micrometers (25 mg/ml DHB in 50% methanol, 10% ammonium acetate, 0.3% trifluoroacetic acid in water; 5 drops per pass and 25 passes).

The MALDI imaging mass spectrometry was performed on an Ultraflex II MALDI TOF/TOF (Bruker Daltonics, Germany) in reflector mode. External calibration was performed with a standard peptide mix (Peptide Standard Calibration II, Bruker Daltonics). Baseline correction (Convex Hull) was performed for each individual spectrum and was exported as dat-files using FlexAnalysis (Bruker Daltonics). Spectra of the mass range from m/z 440 to 8660 were acquired from each matrix spot consisted of 600 laser shots per spot in 20 steps random pattern. Total ion current normalization was performed on each individual spectrum and data quality assessed as previously described (Karlsson et al., 2014). A total of 5400 peaks with a signal-to-noise ratio >3 were selected and peak borders were defined by binning analysis using mass spectrometry peak binning software pbin. The peak area was

calculated for each peak using an in-house developed R script. Data is expressed as average peak area for 40-50 mass spectra collected from the NAc of each mouse (761 spectra in total collected from the NAc of cKO, n=6 and Ctrl, n=3 mice). To specify the anatomical localization of peptides, photomicrographs of matrix deposits were co-registered with histological staining of the same sections. After MS acquisition the matrix was removed with 95% ethanol and the mouse brain sections were stained with toluidine blue (Göteborgs Termometerfabrik AB, Sweden). FlexImaging 2.0 was used for visualization of peptide distribution. F-test analysis of variance revealed unequal variance between groups and the data was log-scaled for further analysis using Student's T-test (two-tailed, alpha 0.05, the null hypothesis was rejected at $P < 0.05$).

*In situ hybridization analyses*

Radioactive *in situ* hybridization was performed as described in (Schweizer et al., 2014) using antisense oligonucleotide probes for detection of Vglut2 mRNA (two independent probes, one composed of a mix of 3 oligonucleotides (NM_080853.3: bases 13-47 (exon1); bases 872-908 (exon 1,2); bases 3220-3254 (exon 12)) and a second probe specific for exon 5 (bases: 1432-1464)) mRNA, respectively, and Pdyn (NM_018863.4 : 1078-1112; 1694-1727; 2309-2342). Images (Fujifilm BioImaging Analyzer BAS-5000, exposure time 1 month) corresponding to hybridized sections were exposed on film for mRNA expression analysis at a 25µm resolution. For cellular mRNA expression analysis, slides were dipped in NTB emulsion, revealed after an exposition of 6 weeks and sections counterstained with toluidine blue. For fluorescent detection, sections were incubated with HRP-conjugated anti-DIG antibody at 1/1000. Signal detection was by the TSA™ Kit (Perkin Elmer) using Biotin-tyramide at dilution 1:75 followed by incubation with Neutravidin Oregon Green conjugate at 1:750. HRP-activity was stopped by incubation of sections in 0,1M glycine followed by a 3% $H_2O_2$ treatment. Fluorescein epitopes were then detected with HRP conjugated anti-

Fluorescein antibody at 1:1000 dilution and revealed with TSA™ Kit (Perkin Elmer) using Cy3 tyramide at 1:200. All slides were scanned on a x40 resolution NanoZoomer 2.0-HT (Hamamatsu, Japan). Cell size measurement, silver grain (mRNA expression) and cell counting were performed using the ndp.view software (Hamamatsu, Japan). Histograms and scatter plots were produced with MATLAB plotting tools (The Mathworks, USA).

*Analysis of projection patterns*

*Vglut2*$^{wt/wt;Pitx2\text{-}Cre+}$ mice (n=6) older than 8 weeks received 5 mg/kg carprofen prior to being anesthetized with isoflurane (0.5-2%). Bilateral stereotactic injections of AAV-DJ.Ef1a.DIO.ChR2(H134R).EYFP.IRES (1 x $10^{12}$ vector genome/mL, UNC Vector Core Facility, USA) were carried out at AP, -1.9 from bregma, ML, ±1.7 from midline. In each hemisphere, 250 nl were injected at DV, -4.75 and -4.25 with a NanoFil syringe with 35-gauge needle (World Precision Instruments, USA) at a rate of 100 nl/min. The needle was left in place for 10 minutes after the second injection and afterwards slowly removed. Injected mice were kept in their home cage for at least 5 weeks to allow EYFP detection in synaptic terminals. Afterwards, the injected mice were anesthetized with isoflurane and decapitated. The brain was removed and kept for 24 h in 4% formaldehyde solution. Coronal sections of 100 µm were prepared on a VT1200 Vibratome (Leica Microsystems, Germany) and mounted in 90% Glycerol. Images were taken on a Leica CTR 6000 microscope and analyzed with LAS AF lite (Leica Biosystems, Germany).

*Histological analysis of STN structure*

3D reconstruction was obtained with MATLAB 3D plotting tools (The Mathworks, USA). 16 and 27 images of KO and WT sections respectively were used to draw contours of the STN. These images were previously adjusted so that adjacent sections fit the best to the real spatial position. We applied 3D cubic spline interpolation for missing sections and standard 'box' smoothing. Different transparency, light shedding and shading options enabled visualization of 3D shape of the STN.

## Results

*Vglut2 and Pitx2 mRNAs overlap and are both distributed over the entire STN*

The STN in both primates and rodents have been suggested to constitute a tripartite structure composed of a dorsal motor aspect with efferent projections to the globus pallidus *interna* (GPi; in mice known as the entopeduncular nucleus, EP) and *externa* (GPe; in mice commonly referred to only as globus pallidus, GP); a ventral aspect which via projections to the substantia nigra *pars reticulata* (SNr) regulates associative behavior; and a medial aspect which communicates with the limbic system via the ventral pallidum (VP) (Kita and Kitai, 1987; Groenewegen and Berendse, 1990; Benarroch, 2008; Alkemade and Forstmann, 2014). While this model is based on projection patterns and functional outcome, no genetic marker has been identified that distinguishes between these three aspects of the STN.

The *Vglut2/Slc17a6* gene encoding the synaptic protein VGLUT2 is strongly expressed (mRNA) within the cytoplasm of neurons located in the STN in both rodents and primates (Hisano, 2003; Barroso-Chinea et al., 2007; Rico et al., 2010) and represent the major glutamatergic population within the STN in mice (Schweizer et al., 2014). For this reason, we wished to assess the distribution pattern of the *Vglut2/Slc17a6*-expressing neurons within the mouse STN to analyze if these distribute differently within the dorsal, ventral and medial aspects of the STN. High-resolution radioactive Vglut2 mRNA-selective *in situ* hybridization analysis was performed to enable visualization and subsequent quantification of Vglut2 mRNA. Vglut2 mRNA, detected as silver grains, was readily visible across the entire extent of the STN (***Fig. 1A left***). While Vglut2 mRNA was present throughout all aspects of the STN, the level of expression was visibly higher in the medial and ventral parts. While most cells contained Vglut2 mRNA, cells of different sizes appeared throughout the STN (***Fig. 1A, right***).

316 Further, because the *Pitx2* gene has been shown to be highly expressed in the STN (Martin
317 et al., 2004), we next used double fluorescent *in situ* hybridization to analyze the distribution
318 also of Pitx2 mRNA, as well as the overlap between Vglut2 and Pitx2 mRNA on a cellular
319 level. Throughout all aspects of the STN, a near-100% overlap between these two mRNAs
320 was observed (***Fig. 1B***). The distribution pattern of both Vglut2 and Pitx2 mRNA was
321 important to establish since we, as discussed above, use a *Pitx2-Cre* transgenic mouse line
322 (Skidmore et al., 2008) as a tool to enable targeted deletion of *Vglut2/Slc17a6* expression
323 within the STN (Schweizer et al., 2014). However, we had not previously addressed the
324 possibility of subregional targeting within this structure. Our previous analysis showed that
325 the $Vglut2^{f/f;Pitx2\text{-}Cre+}$ conditional knockout (cKO) mice and their control littermates
326 ($Vglut2^{f/f;Pitx2\text{-}Cre-}$) as expected had similar levels of Pitx2 mRNA in the STN. However,
327 *Vglut2/Slc17a6* expression levels were blunted in the cKO STN so that the amount of low-
328 level expression cells were increased at the expense of high-level expression cells, leaving a
329 40% decrease in Vglut2 mRNA (Schweizer et al., 2014).

330 Having now assured that *Pitx2* and *Vglut2/Slc17a6* expressions were overlapping and
331 distributed all over the STN, we next quantified the amount of Vglut2 mRNA by counting the
332 number of silver grains in 550 STN neurons of cKO and 792 of the control mice, respectively.
333 About 12% of all the counted STN neurons in the control mice lacked any detectable Vglut2
334 mRNA, while the remaining approximately 88% of STN neurons showed of wide range of
335 Vglut2 mRNA expression levels (***Fig. 1C***). The number of cells expressing no detectable
336 Vglut2 mRNA at all was more than double throughout the STN structure in the cKO
337 compared to control (28% *vs* 12%). Further, the number of low level Vglut2 mRNA levels (1-
338 10 silver grains/cell) was higher in the cKO than control STN while more control than cKO
339 STN cells showed higher Vglut2 mRNA levels (11 or more silver grains/cell).

These histological analyses show that in the mouse, Pitx2 and Vglut2 mRNAs are highly overlapping (near-100%) throughout the extent of the STN and thus do not represent any specific aspect of the STN. Moreover, in control mice, as much as almost 90% of all STN neurons express the *Vglut2/Slc17a6* gene while the majority of cKO neurons in the STN contain no or low levels of Vglut2 mRNA. Thus, the current results demonstrate that *Vglut2/Slc17a6* expression levels are severely blunted throughout the entire STN structure of the *Vglut2*$^{f/f;Pitx2\text{-}Cre+}$ (cKO) mice.

*Normal reward-associated learning, memory and cognitive flexibility but lower sugar consumption when* Vglut2/Slc17a6 *expression is blunted within the STN*

Hyperactive individuals, mice as well as humans, can be lean without having any kind of deficiency in food consumption. Therefore, the slightly smaller size of the hyperactive cKO mice did not appear abnormal at first, but since a lower rate in collecting high-fat food pellets in the baited radial arm maze and in the delay discounting test was measured (Schweizer et al., 2014), a more thorough analysis of feeding behavior was motivated.

Generally, decreased consumption of fatty food might reflect a decreased eating overall or a lack of consumption of palatable eatables specifically, the latter which could reflect a deficiency in the mesostriatal reinforcement system (Everitt and Robbins, 2005), also known as the brain reward system. To differentiate between these two possibilities, voluntary consumption of high-sucrose food, another palatable eatable, was assessed in an operant self-administration paradigm (Skinner, 1966) under mild food-restriction (***Fig. 2A***, schematic presentation of the entire experiment; 2***B***, illustration of the operant chamber). The results of this analysis showed that no difference between control and cKO groups could be observed in task acquisition (training) as both groups learned equally well to collect the maximum of 30 pellets and decreased the time for task completion during training (change over time: p=<0.0001; F=13.16 Df=3) (***Fig. 2C***). Both groups were able to reliably collect 30 pellets on three

consecutive days on the FR1 schedule (***Fig. 2D, left and middle***). However, the time to complete the FR1 task was significantly increased for cKO mice compared to controls (variation between genotypes: p=<0.0001; F=23.58; Df=1) (***Fig. 2E, left***). Furthermore, the control mice continued to increase the number of head entries during time-out over the trial while the number of head entries of cKO mice declined (time x genotype: p=0.00113; F=5.024; Df=2) (***Fig. 2D, right***). During FR5, the control mice showed a higher number of head entries than cKO mice when a pellet could be obtained (time x genotype: p=0.0336; F=2.802, Df=4; variation between genotypes: p=0.0076; F=9.476; Df=1) (***Fig. 2E, left***), thus leading to a higher consumption of sugar pellets (time x genotype: p=0.0336; F=2.802; Df=4; variation between genotypes: p=0.0076; F=9.476; Df=1) (***Fig. 2E, middle***). In addition, cKO mice displayed decreased seeking for sugar during time-out in the FR5 paradigm (variation between genotypes: p=0.0175; F=7.012; Df=1) (***Fig. 2E, right***).

While FR5 is used to measure sugar consumption rate, the PR paradigm has been described as a measure for the motivational aspect of consumption (Sanchis-Segura and Spanagel, 2006). During PR, the number of head entries when the feeder was active (time x genotype: p=0.3776; F=0.9992; Df=2) or during time-out (time x genotype: p=0.1506; F=1.986; Df=2) was similar between cKO and controls (***Fig. 2F***). A breaking point was not observed in either group. During the extinction phase, both groups decreased their number of head entries at a similar pace (change over time: p=<0.0001; F=45.24; Df=4; variation between genotypes: p=0.9457; F=0.0049; Df=1) (***Fig. 2H, left***). Head entries during time-out decreased as well (time x genotype: p=0.0085; F=4.105; Df=4; change over time: p= <0.0001; F=130.2; Df=4; variation between genotypes: p=0.2763; F=1.365; Df=1) with head entries in cKO only significantly lower on the first day (Post-hoc test with Bonferroni correction, p<0.01; t=3.736) but not the other days (***Fig. 2H, right***). Upon reinstatement of the operant task, control and cKO groups showed no difference in the level of activity at the

active feeder (p>0.05) and were also equally able to switch sides upon reversal of the active and inactive feeders (time x genotype: p=0.0015; F=4.005; Df=6; change over time: p=0.0014; F=7.172; Df=2) (***Fig. 2I***). Throughout the experiment, activity on the inactive feeder was low in both the control and cKO groups (***source data Figure 2-1***).

Analysis of operant sugar consumption behavior thus demonstrates that while the cKO mice displayed normal reward-related learning, motivation, memory and ability for task-switching, their consummatory rate of sugar eatables was significantly reduced.

*Lower weight but normal re-feeding after food restriction*

During the whole self-administration regime, mice were weighed daily to control for body weight fluctuations. This procedure showed that the cKO mice weighed less than controls throughout the trial but that cKO and control mice followed the same overall shifting in weights between days (time x genotype: p= 0.0011; F= 2.860; Df=12) (***Fig. 3A***). Upon completion of the self-administration task, all mice were allowed to feed freely in their home cage environment (re-feeding). Despite weight difference, both control and cKO mice consumed similar amounts of standard rodent chow during re-feeding (time x genotype: p=0.6323; F=0.6911; Df=5) (***Fig. 3B***).

As the cKO mice consumed normal amounts of standard chow during re-feeding after the operant task, the results suggest that the observed effect on sugar consumption is specific to sweet food and that the leaner shape of the cKO mice prior to food-restriction rather reflects their hyperactivity than a deficiency in standard chow feeding.

*Significant increase in seated and free rearing corroborates elevated motor activity*

*Vglut2*$^{f/f;Pitx2\text{-}Cre+}$ cKO mice are both vertically and horizontally hyperactive (Schweizer et al., 2014). By showing that they consume less sugar, we wished to know more about their motor behavior. Rearing behavior differs from locomotion as is does not serve to move the mouse forward, but instead signifies a sensing of the environment, commonly interpreted as

an exploratory behavior. Further, rearing displayed in a repetitive format is commonly interpreted as a form of stereotypy in rodent models of various neuropsychiatric disorders (Kim et al., 2016). It has also been shown that the presentation of rearing behavior in mice can appear in different ways depending on body posture and the positioning of the paws and tail (Waddington et al., 2001). To explore the type of rearing accentuated in the *Vglut2*$^{f/f;Pitx2\text{-}Cre+}$ cKO mice, we analyzed it in detail by sub-categorizing rearing into the three different subtypes; wall rearing (***Fig. 4A, left***), seated rearing (***Fig. 4B, left***), and free rearing (***Fig. 4C, left***), as previously described (Waddington et al., 2001). By quantifying the duration of each of the types of rearing, no significant difference in wall rearing was found between control and cKO mice (variation between genotypes: p=0.2577; F=1.441; Df=1) (***Fig. 4A, right***). In contrast, both seated rearing (interaction: p=0.0127; F=5.625; Df=2) (***Fig. 4B, right***) and free rearing (p=0.0081; F=6.366; Df=2) (***Fig. 4C, right***), the two more complex forms of rearing, were significantly over-represented in the *Vglut2*$^{f/f;Pitx2\text{-}Cre+}$ cKO group of mice (***Fig. 4***).

Summarizing the behavioral findings, the results demonstrate that mice lacking normal expression levels of the *Vglut2/Slc17a6* gene in the STN display severely elevated motor activity, including advanced subtypes of rearing barely detected in control mice, and blunted reward consumption. These findings suggest an over-activity of the motor system at the expense of the reward system, a finding which next motivated analysis of the mesostriatal dopamine (DA) system.

*Significant alterations in DA receptor and DA transporter capacity*

DA neurotransmission in the dorsal striatum, mediated by the nigrostriatal DA neurons located in the substantia nigra *pars compacta* (SNc), is strongly correlated with locomotion and rearing, while DA transmission in the nucleus accumbens (NAc), the ventral aspect of the striatum, is primarily mediated by DA neurons of the ventral tegmental area (VTA) and is triggered by palatable food and drugs of abuse (Björklund and Dunnett, 2007). The reduced

interest in palatable food rewards alongside the elevated motor behavior thus suggested an opposing circuitry effect by the targeted deletion of the *Vglut2/Slc17a6* gene in the STN on dorsal and ventral striatal DA signaling. Indeed, in our previous analyses, we showed that the nigrostriatal DA system is over-active with increased levels of DA release and reduced DA clearance due to reduced levels of the DA transporter (DAT) in the DStr, while no alteration in terms of DA receptor availability was detected (Schweizer et al., 2014).

Having now unraveled an effect of the *Vglut2*-targeting of the STN on consumption of natural rewards, we focused on addressing a possible contribution of the NAc. The levels of DA receptors are important for the hedonic impact of drugs of abuse and palatable food (Volkow et al., 1999; Wenzel and Cheer, 2014). We therefore implemented receptor autoradiography of [$^{3}$H]SCH23390, [$^{125}$I]iodosulpride and [$^{125}$I]7-OH-PIPAT bindings (Mahmoudi et al., 2014) to measure the density of DA receptor D1R, D2R and D3R subtypes, respectively (***Fig. 5A***). No difference between control and cKO mice was detected for D1R in either the core or shell subregions of the NAc (NAcC and NAcSh, respectively) (***Fig. 5B***). However, for both D2R and D3R, ligand binding was altered in the NAcSh. D2R binding was elevated above control levels in the cKO brain while D3R ligand binding was decreased (***Fig. 5C and D***). In addition, D2R binding was also above control levels in the cKO NAcC (***Fig. 5D***). Next, we assessed DAT capacity using [$^{125}$I]RTI-121 binding. [$^{125}$I]RTI-121 binding was significantly increased in the NAcSh (***Fig. 5E***).

These findings point to different, and even opposite, modifications in the dorsal versus the ventral striatal DA systems upon the targeted deletion of *Vglut2* in the STN such that the NAcSh of the cKO mice have altered D2R and D3R availability as well as increased DAT capacity, as opposed to unaltered receptor state and decreased DAT capacity in the dorsal striatum (Schweizer et al., 2014). The higher activity of the dorsal over the ventral striatal DA system likely accounts for the observed strengthening of motor behavior and weakening of

the natural reward-related behavior, and with focus on the reward system, the NAc was therefore analyzed in more detail.

*Altered levels of dynorphin neuropeptide, but not gene expression, in the NAc*

To enable analysis of the molecular constitution within the neurons of the NAc and to assay for peptide alterations within this region of Vglut2$^{f/f;Pitx2\text{-}Cre+}$ cKO and control mice, we implemented Matrix-assisted laser desorption/ionization analysis (MALDI) imaging as previously described (Hanrieder et al., 2011; Ljungdahl et al., 2011) (**Fig. 6A** schematic illustration of the procedure). The unknown peptides with mass to charge ratio (m/z) 1835 and m/z 1393 were used to visualize white matter fiber tracts and the striatum, respectively, serving as landmarks for the localization of the NAc (**Fig. 6B**).

The majority of over hundred detected peptides detected in the MALDI imaging were not differentially expressed in cKO and control animals. However, 19 peaks were significantly downregulated and 48 upregulated in the cKO mice. Among these upregulated peptides, the strong changes in the family of dynorphin (Dyn) neuropeptides were most striking. Ion images for the Dyn peptides DynA and alpha-neoendorphine (aNeo) revealed visibly elevated Dyn levels in the NAc (**Fig. 6B**). Ion images obtained from cKO mice exhibited 25 to 50% higher levels of Dyn and aNeo peptides compared to control mice. These alterations were mainly localized to the NAc (**Fig. 6C**). Dyn peptides including DynB (9-13; p=0.0290), DynB (1-6; p=0.0087), DynB (2-13; p=0.0334), aNeo (p=0.0196 for first and p=0.0352 for second isotope), aNeo (2-10; p=0.0289), and DynA (p=0.0021) were upregulated in the NAc of the cKO compared to the control brains (**Fig 6D**). The Dyn neuropeptides are products generated by prohormone convertase cleavage of the prodynorphin (Pdyn) propeptide (Berman et al., 2000; Yakovleva et al., 2006; Orduna and Beaudry, 2016), and while Dyn peptides can represent either afferent or local projections, expression of the *Pdyn* gene was next analyzed at mRNA level by in situ hybridization in the NAc. No difference in expression between

control and cKO could be detected, suggesting that the regulation of the Pdyn peptide products does not occur at mRNA but at the peptide level (**Fig. 6F**).

Taken together with the results from the DA receptor and DAT binding shown above, these findings reveal that the targeted reduction of Vglut2 within the STN had a strong impact on the mesostriatal DA reward system, and we sought to explore this correlation further.

*Pitx2-Cre-expressing STN neurons show unique projection patterns to EP/GP and SNr*

The STN has been reported to send a multitude of efferents to the basal ganglia and their associated structures, including the GPi/EP, GPe/GP, SNr, VP, pedunculopontine nucleus (PPN), SNc and basolateral amygdala (BLA) (Kita and Kitai, 1987; Parent and Hazrati, 1995; Parent et al., 2000; Sato et al., 2000; Benarroch, 2008; Degos et al., 2008; Watabe-Uchida et al., 2012; Hachem-Delaunay et al., 2015). However, to our knowledge, no direct innervation from the STN to either the NAc or DStr has so far been identified. While we already confirmed a strongly reduced glutamatergic activity by implementing patch-clamp recordings both upon electrical and optogenetic stimulations in post-synaptic neurons in the main STN target areas EP and SNr (Schweizer et al., 2014), we now aimed to establish if there is a projection from *Pitx2/Vglut2* co-expressing STN neurons directly to the NAc, which could explain the strong effects observed in this region of the cKO mice. To selectively trace the efferent projections and thereby pin-point their target areas, an adeno-associated virus (AAV) carrying a Cre-dependent DNA construct of the *Channelrhodopsin-2* (ChR2) gene and the gene encoding the Enhanced yellow fluorescent protein reporter (EYFP) was stereotactically injected bilaterally into the STN of control $Vglut2^{wt/wt;Pitx2\text{-}Cre+}$ mice (***Fig. 7A-B***). Virus was injected in two different dorsal-ventral stereotactic STN coordinates to ensure expression throughout the length of the STN (***Fig. 7C***). Histological analysis revealed absence of EYFP in structures surrounding the STN, while ample EYFP-positive cell bodies were detected throughout the extent of the STN, confirming both successful expression of the *ChR2-EYFP*

construct exclusively in the *Pitx2-Cre*-expressing neurons and the observation described above that *Pitx2/Vglut2* co-expressing cells are distributed uniformly over this structure (***Fig. 7D***). The EP, GP and SNr were verified as targets of the *Pitx2-Cre*-expressing STN neurons by EYFP localized to fibers throughout these areas (***Fig. 7E-G***). However, no EYFP-positive innervation at all could be detected in either the NAc or in the DStr (***Fig. 7H***). Further, EYFP could not be detected in any of the other target areas described for the STN in different species, i.e. the SNc, VP, BLA and PPN (***Fig. 7H***).

The results of these tracing studies thereby show that the alterations observed on the DA parameters in the NAc are most likely mediated via the already established target areas of the *Pitx2/Vglut2* co-expressing neurons, i.e. EP, GP or SNr, and not via a direct projection from the STN to the NAc. To further explore how the *Vglut2*-targeting of the STN might have caused the striatal alterations observed, we next sought to explore if the targeted blunting of *Vglut2/Slc17a6* gene expression might have caused any alterations in the structure of the STN that might contribute to the dopaminergic phenotype observed.

*Cell loss as well as altered structural size and shape of the STN*

A previous study of dopamine-glutamate co-releasing neurons in the midbrain has shown that expression of the Vglut2/Slc17a6 gene is important for maintaining cell density (Fortin et al., 2012). During visual inspection of cryosectioned brains, we had detected a difference in the shape of the STN between cKO and control mice and for this reason we decided to quantify cell density and to also measure the size and shape of the STN. Toluidine blue-contrast staining of the serially sectioned control and cKO mice used to quantify Vglut2 mRNA described above enabled quantification of cell number and cell size (area) in the same material. This analysis revealed a reduction in total number of cells by 39% in the cKO compared to control. Further, more STN neurons in the cKO than control mice had larger cell area (201-350 $\mu m^2$), leading to right-sided shift in the histogram presenting cell area as a

function of % of total cells (**Fig. 8A**). It was also evident that within the STN of cKO mice, there are neurons of a larger size range (351-500 $\mu m^2$) than observed at all in the control STN.

We next analyzed if the overall structure of the STN in the cKO mice had been altered as a consequence of this cell loss. For this task, 2D and 3D reconstruction analyses were performed in parallel. For 2D analysis, anatomical outlines of the STN were made on each section microscope photograph and linear measurements were made at the widest part of the STN and the adjacent cerebral peduncle (**Fig. 8B-C**). These analyses revealed that the STN was slimmer in the cKO than in the control animals while the cerebral peduncle was wider, thus pointing to shrinkage of the STN in the cKO. The STN outlines were subsequently used to establish 3D overlay pictures of cKO and control STN both from coronal and sagittal view, both of which readily exposed the smaller size of the STN in the cKO mice (**Fig. 8D**). Further, the ventral and dorsomedial aspects of the STN were exposed as the regions most affected by the reduction in STN size and this led to a change in the overall shape of the STN which appeared visibly narrower ventrally and dorsomedially (**Fig. 8D**). 3D-quantification confirmed a 14% smaller diameter as well as a 38% reduction in volume in the cKO STN.

These results demonstrate that the targeted deletion of the Vglut2/Slc17a6 gene in the STN causes substantial loss of neurons, primarily those of small cell area, which in turn likely has caused the alteration in the size as well as shape of the entire STN structure. This substantial alteration likely contributes to the motor and reward behavioral alterations observed. Further, the results obtained pinpoint Vglut2/Slc17a6 gene expression levels as crucial for the structure and function of the STN.

## Discussion

The STN has gained wide attention based on its pivotal role in motor, limbic and cognitive functions and therapies based on electrical brain stimulation of the STN show a steady increase as a treatment of advanced PD and a range of neuropsychiatric disorders (Chabardès et al., 2013). Aberrant excitation from the STN not only contributes to the core symptoms of PD, i.e bradykinesia, rigidity, tremor and axial instability, but excessive excitation from the STN has also been proposed to also contribute to the degeneration of midbrain DA neurons and may thus play a role in the etiology of this disease (Rodriguez et al., 1998; Olanow and Tatton, 1999; Menegas et al., 2015).

While the so called tripartite model of the STN dominates the current way of correlating the anatomy of the STN with its many functional roles, this model has recently been challenged (Keuken et al., 2012; Alkemade and Forstmann, 2014; Lambert et al., 2015). Interestingly, no molecular markers have been identified that could be used to delineate putative anatomical borders between the three main subdivisions of the STN; this lack of subdivision-selective markers contributes, in our mind, to the difficulty in firmly confirming or dismissing the tripartite model. Both Vglut2 and Pitx2 mRNAs localize within the mouse STN (Martin et al., 2004; Schweizer et al., 2014) but the current study shows that they are both distributed throughout the entire STN structure; neither Vglut2 or Pitx2 can thus serve as a selective marker for any specific aspect within the STN. We further conclude that while we already previously referred to the *Pitx2/Vglut2* co-expressing neurons as a subpopulation of the STN (Schweizer et al., 2014), the demonstration that Pitx2 and Vglut2 mRNA overlap in almost 90% of all STN neurons now pin-points that the *Pitx2/Vglut2* subpopulation represent the vast majority of the STN.

Given this broad distribution of Vglut2 and Pitx2 mRNAs throughout the STN, and the reduction of Vglut2 mRNA levels throughout the STN structure of the *Vglut2*$^{f/f;Pitx2\text{-}Cre+}$ cKO

586 mice, a strong behavioral phenotype might not be surprising. The surprise, if any, rather lays
587 in the seemingly opposing effects observed on motor and reward-related behavior. While
588 motorically hyperactive both vertically and horizontally, the cKO mice consume less sugar
589 than control mice. Previous studies in rats selected for their low (LRA) or high (HRA) rearing
590 activity have shown that HRA rats display elevated locomotor activity and collect rewards in
591 the baited radial arms maze faster than LRA rats, but as they also make more working
592 memory errors, these results suggested that higher reward consumption in hyperactive rodents
593 is correlated with working memory failure (Görisch and Schwarting, 2006). While the
594 *Vglut2*$^{f/f;Pitx2\text{-}Cre+}$ cKO mice previously were shown to be strongly hyperactive both in terms of
595 locomotion and rearing, they did not make more errors in the baited radial arm maze; neither
596 reference or working memory errors were elevated in the cKO mice (Schweizer et al., 2014;
597 Pupe et al., 2015). However, consistently throughout our natural reward-related tests, i.e. the
598 baited radial arm and delay discounting tests as well as the sugar self-administration presented
599 here, the *Vglut2*$^{f/f;Pitx2\text{-}Cre+}$ cKO mice consumed less than controls.

600 Based on these observed behavioral alterations, we argue that the motoric hyperactivity
601 overrides the interest in palatable food. In efforts to unravel the biochemical correlates of such
602 a behavioral phenotype, we identified a series of modifications that support this argument.
603 First, a strong correlation between DA signaling in the NAcSh and reward-related behaviors is
604 already well established (Everitt and Robbins, 2005) and dysfunction of the mesostriatal DA
605 system is strongly implicated in disorders with a reward-related component, including
606 addiction (Volkow et al., 2009), anorexia nervosa (Kontis and Theochari, 2012) and over-
607 eating (Wang et al., 2001; Stice et al., 2008). By now demonstrating that the targeting of
608 *Vglut2/Slc17a6* gene has caused an increase in the DA activity in the DStr (mainly motor) but
609 decreased it in the NAc (mainly reward), opposite behavioral outcome mediated by these two
610 systems might indeed be achieved. The selective lack of interest in palatable food, while

showing normal levels of regular chow consumption, is likely correlated to the biochemical alterations in the NAc. Increased DAT capacity suggests faster clearance of DA while the elevated levels of Dyn peptides might represent a biochemical indication for a dysphoric state in these animals.

Microinjection of the selective κ opioid receptor agonist DAMGO in the NAc of experimental animals has previously been shown to produce conditioned place aversion (Bals-Kubik et al., 1993), while an antagonist of these receptors causes an anti-depressant effect (Shirayama and Chaki, 2006). The Dyn neuropeptides are mainly present in D1R-expressing cells of the NAcSh (Al-Hasani et al., 2015); although we did not observe D1R upregulation, the observed reduction in binding to D3R, which can oppose D1R activity, could have relieved D1R intracellular signaling to increase Dyn levels in the NAc (Schwartz et al., 1998). Thus, while elevated motor activity might be explained by the observed reduction of glutamatergic post-synaptic activity in the EP and SNr alongside the reduced DAT clearance in the DStr observed in the *Vglut2*$^{f/f;Pitx2\text{-}Cre+}$ cKO mice, the current findings of elevated DAT levels in the NAcSh as well as increased levels of both D2R and Dyn neuropeptides likely provide a biochemical correlate of the deficiency in the reward-collecting behavior demonstrated by the *Vglut2*$^{f/f;Pitx2\text{-}Cre+}$ cKO mice. Further, by unraveling the severe impact on the size and shape of the STN structure itself, we propose that slimming of the ventral (presumably associative) and part of the medial (limbic) aspects of the STN due might cause the reduced dopaminergic activity in the NAc. Similar slimming of the STN structure has been observed upon ibotenic acid-induced STN lesioning in which a substantial amount of STN cells are lost (Baunez et al., 1995, 2002), while targeted deletion of the *Vglut2/Slc17a6* gene in the midbrain has been shown before to lead to reduced cell density (Fortin et al., 2012).

In the *Vglut2*$^{f/f;Pitx2\text{-}Cre+}$ cKO mice, expression of the *Vglut2/Slc17a6* gene is targeted from early embryogenesis and onwards. Having now verified that reduced Vglut2 mRNA levels

636 occur throughout the STN structure, and also shown that the STN suffers from cell loss and
637 structural modifications, this genetic intervention resembles to some extent a pharmacological
638 lesion model of the STN. Indeed, pharmacological lesioning, as well as inactivation, of the
639 STN increases motoric activity and have also been shown more recently to affect motivated
640 behavior, including consumption of palatable food (Baunez et al., 2002, 2005; Bezzina et al.,
641 2008; Rouaud et al., 2010). While pharmacological lesioning and inactivation of the STN, as
642 well as STN-DBS, in experimental animals show similar beneficial effects on motor behavior
643 as STN-DBS in humans (Baunez and Gubellini, 2010), the results have been more variable
644 and difficult to interpret in terms of motivated and reward-related behavior; this is likely due
645 to the use of different experimental paradigms and to the metabolic states of animals (e.g.
646 food-restriction) analyzed in the reported studies (Uslaner et al., 2007; Pratt et al., 2012).
647 Importantly, the *Vglut2/Slc17a6* "genetic lesion model" (represented by the *Vglut2*$^{f/f;Pitx2\text{-}Cre+}$
648 cKO mice) has a developmental onset which sets it aside from current pharmacological
649 lesion models. In the *Vglut2*$^{f/f;Pitx2\text{-}Cre+}$ cKO mice, the there is a significant reduction in
650 number of the STN neurons in the adult animal, which in turn likely has caused the alteration
651 in STN shape. However, addressing dysfunction in developmental processes, such as defects
652 in proliferation or premature cell death, is beyond the scope of the present study. Further,
653 STN neurons may not differentiate or migrate in a normal manner and they may not even
654 form functional connections in the absence of normal levels of *Vglut2/Slc17a6* gene
655 expression.
656 The impact of a developmentally-induced "genetic lesion" likely has a substantial effect of
657 overall circuitry. Therefore, identifying the exact nature of the correlation between the
658 reduced *Vglut2/Slc17a6* gene expression levels, the altered shape of the STN and the observed
659 effects on the DA system is not straight-forward. While we can conclude that there is no direct
660 innervation of either the ventral or dorsal striatum by the *Pitx2/Vglut2* co-expressing STN

neurons that might be directly affected by the targeted deletion of *Vglut2/Slc17a6*, we have established that both the EP and SNr are innervated by these STN neurons, and that the glutamatergic input into these targets is reduced in the *Vglut2*$^{f/f;Pitx2\text{-}Cre+}$ cKO mice. The EP is the main projection target in the STN motor loop while the SNr also mediates associative functions (Benarroch, 2008), and we therefore hypothesize that the observed alterations in reward-related behavior might be connected more specifically to the STN-SNr pathway. While STN neurons generally are excitatory in nature, high-frequency stimulation of the STN leads to a reduced drive for burst firing in the SNr (Shen and Johnson, 2008) and can through endocannabinoid mechanisms attenuate the GABAergic innervation of the SNc through the SNr (Freestone et al., 2015). The reduction in glutamatergic transmission in the STN of the *Vglut2*$^{f/f;Pitx2\text{-}Cre+}$ cKO could therefore have led to a developmental alteration in the excitation/inhibition balance within the STN-SNr-SNc axis, presumably via the structurally disturbed ventral and part of the medial aspects of the STN.

Developmental effects might make it difficult to pinpoint additional circuitry components in the STN-EP/GP/SNr-striatum-loop unraveled here. However, targeting the *Vglut2/Slc17a6* gene bears a physiological relevance that is not matched by toxin-induced models. Null mutations of the *Vglut2/Slc17a6* gene in mice are lethal directly after birth due to disturbance of the pre-Bötzinger respiratory central pattern generator (Wallén-Mackenzie et al., 2006) and the same is likely true for humans. However, some rare genetic variants of the human VGLUT2/SLC17A6 gene have been identified in schizophrenia and severe alcoholism (Flatscher-Bader et al., 2008; Shen et al., 2010; Comasco et al., 2014). In the *Vglut2*$^{f/f;Pitx2\text{-}Cre+}$ cKO mice, expression levels of the *Vglut2/Slc17a6* gene are merely blunted, but not eliminated, and may therefore expose effects that are of relevance to human conditions. Indeed, we show that the blunting of *Vglut2/Slc17a6* gene expression levels selectively within the STN of mice cause opposite biochemical modifications in the dorsal and ventral striatal

DA systems followed through by behavioral hyperactivity and decreased interest in palatable food, possibly due to a dysphoric state. We tentatively propose that genetic variants of the human VGLUT2/SLC17A6 gene might be correlated with similar modifications. Further, by demonstrating an association between reduced Vglut2 mRNA levels in the STN and reduced STN size in mice, brain imaging analysis of STN size in human individuals might serve a purpose in future clinical investigations of human brain disorders implicating the STN, and where STN-based therapies are implemented already, such as PD and OCD, as well as for addiction, eating disorders and obesity, disorders proposed to benefit from STN-based therapy.

## References


Al-Hasani R, McCall JG, Shin G, Gomez AM, Schmitz GP, Bernardi JM, Pyo CO, Park SI, Marcinkiewcz CM, Crowley NA, Krashes MJ, Lowell BB, Kash TL, Rogers JA, Bruchas MR (2015) Distinct Subpopulations of Nucleus Accumbens Dynorphin Neurons Drive Aversion and Reward. Neuron 87:1063–1077.

Alkemade A, Forstmann BU (2014) Do we need to revise the tripartite subdivision hypothesis of the human subthalamic nucleus (STN)? Neuroimage 95:326–329.

Andersson M, Groseclose MR, Deutch AY, Caprioli RM (2008) Imaging mass spectrometry of proteins and peptides: 3D volume reconstruction. Nat Methods 5:101–108.

Bals-Kubik R, Ableitner A, Herz A, Shippenberg TS (1993) Neuroanatomical sites mediating the motivational effects of opioids as mapped by the conditioned place preference paradigm in rats. J Pharmacol Exp Ther 264:489–495.

Barroso-Chinea P, Castle M, Aymerich MS, Perez-Manso M, Erro E, Tunon T, Lanciego JL (2007) Expression of the mRNAs encoding for the vesicular glutamate transporters 1 and 2 in the rat thalamus. J Comp Neurol 501:703–715.

Baunez C, Amalric M, Robbins TW (2002) Enhanced Food-Related Motivation after Bilateral Lesions of the Subthalamic Nucleus. J Neurosci 22:562–568.

Baunez C, Dias C, Cador M, Amalric M (2005) The subthalamic nucleus exerts opposite control on cocaine and "natural" rewards. Nat Neurosci 8:484–489.

Baunez C, Gubellini P (2010) Effects of GPi and STN inactivation on physiological, motor, cognitive and motivational processes in animal models of Parkinson's disease. Prog Brain Res 183:235–258.

Baunez C, Nieoullon A, Amalric M (1995) In a rat model of parkinsonism, lesions of the subthalamic nucleus reverse increases of reaction time but induce a dramatic premature responding deficit. J Neurosci 15:6531–6541.

Benabid AL, Chabardes S, Mitrofanis J, Pollak P (2009) Deep brain stimulation of the subthalamic nucleus for the treatment of Parkinson's disease. Lancet Neurol 8:67–81.

Benarroch EE (2008) Subthalamic nucleus and its connections: Anatomic substrate for the network effects of deep brain stimulation. Neurology 70:1991–1995.

Berman Y, Mzhavia N, Polonskaia A, Furuta M, Steiner DF, Pintar JE, Devi LA (2000) Defective prodynorphin processing in mice lacking prohormone convertase PC2. J Neurochem 75:1763–1770.

Bezzina G, Boon FS d., Hampson CL, Cheung THC, Body S, Bradshaw CM, Szabadi E, Anderson IM, Deakin JFW (2008) Effect of quinolinic acid-induced lesions of the subthalamic nucleus on performance on a progressive-ratio schedule of reinforcement: A quantitative analysis. Behav Brain Res 195:223–230.

Björklund A, Dunnett SB (2007) Dopamine neuron systems in the brain: an update. Trends Neurosci 30:194–202.

734 Blomstedt P, Sjöberg RL, Hansson M, Bodlund O, Hariz MI (2013) Deep brain stimulation in
735 the treatment of obsessive-compulsive disorder. World Neurosurg 80:e245–e253.

736 Breysse E, Pelloux Y, Baunez C (2015) The Good and Bad Differentially Encoded within the
737 Subthalamic Nucleus in Rats,,. eNeuro 2 Available at:
738 http://www.ncbi.nlm.nih.gov/pmc/articles/PMC4607759/ [Accessed November 24,
739 2015].

740 Chabardès S, Polosan M, Krack P, Bastin J, Krainik A, David O, Bougerol T, Benabid AL
741 (2013) Deep brain stimulation for obsessive-compulsive disorder: subthalamic nucleus
742 target. World Neurosurg 80:S31.e1–e8.

743 Comasco E, Hallman J, Wallén-Mackenzie A (2014) Haplotype-tag single nucleotide
744 polymorphism analysis of the vesicular glutamate transporter (VGLUT) genes in
745 severely alcoholic women. Psychiatry Res 219:403–405.

746 Crusio WE (2004) Flanking gene and genetic background problems in genetically
747 manipulated mice. Biol Psychiatry 56:381–385.

748 Darbaky Y, Baunez C, Arecchi P, Legallet E, Apicella P (2005) Reward-related neuronal
749 activity in the subthalamic nucleus of the monkey. Neuroreport 16:1241–1244.

750 Degos B, Deniau J-M, Le Cam J, Mailly P, Maurice N (2008) Evidence for a direct
751 subthalamo-cortical loop circuit in the rat. Eur J Neurosci 27:2599–2610.

752 Espinosa-Parrilla JF, Baunez C, Apicella P (2013) Linking reward processing to behavioral
753 output: motor and motivational integration in the primate subthalamic nucleus. Front
754 Comput Neurosci 7:175.

755 Everitt BJ, Robbins TW (2005) Neural systems of reinforcement for drug addiction: from
756 actions to habits to compulsion. Nat Neurosci 8:1481–1489.

757 Flatscher-Bader T, Zuvela N, Landis N, Wilce PA (2008) Smoking and alcoholism target
758 genes associated with plasticity and glutamate transmission in the human ventral
759 tegmental area. Hum Mol Genet 17:38–51.

760 Fortin GM, Bourque MJ, Mendez JA, Leo D, Nordenankar K, Birgner C, Arvidsson E, Rymar
761 VV, Berube-Carriere N, Claveau AM, Descarries L, Sadikot AF, Wallen-Mackenzie
762 A, Trudeau LE (2012) Glutamate corelease promotes growth and survival of midbrain
763 dopamine neurons. J Neurosci 32:17477–17491.

764 Freestone PS, Wu XH, de Guzman G, Lipski J (2015) Excitatory drive from the Subthalamic
765 nucleus attenuates GABAergic transmission in the Substantia Nigra pars compacta via
766 endocannabinoids. Eur J Pharmacol 767:144–151.

767 Görisch J, Schwarting RKW (2006) Wistar rats with high versus low rearing activity differ in
768 radial maze performance. Neurobiol Learn Mem 86:175–187.

769 Groenewegen HJ, Berendse HW (1990) Connections of the subthalamic nucleus with ventral
770 striatopallidal parts of the basal ganglia in the rat. J Comp Neurol 294:607–622.

771 Groseclose MR, Andersson M, Hardesty WM, Caprioli RM (2007) Identification of proteins
772 directly from tissue: in situ tryptic digestions coupled with imaging mass
773 spectrometry. J Mass Spectrom 42:254–262.

774 Hachem-Delaunay S, Fournier M-L, Cohen C, Bonneau N, Cador M, Baunez C, Le Moine C
775 (2015) Subthalamic nucleus high-frequency stimulation modulates neuronal reactivity
776 to cocaine within the reward circuit. Neurobiol Dis 80:54–62.

777 Hanrieder J, Ljungdahl A, Falth M, Mammo SE, Bergquist J, Andersson M (2011) L-DOPA-
778 induced dyskinesia is associated with regional increase of striatal dynorphin peptides
779 as elucidated by imaging mass spectrometry. Mol Cell Proteomics 10:M111 009308.

780 Hisano S (2003) Vesicular glutamate transporters in the brain. Anat Sci Int 78:191–204.

781 Karlsson O, Bergquist J, Andersson M (2014) Quality measures of imaging mass
782 spectrometry aids in revealing long-term striatal protein changes induced by neonatal
783 exposure to the cyanobacterial toxin β-N-methylamino-L-alanine (BMAA). Mol Cell
784 Proteomics MCP 13:93–104.

785 Keuken MC, Uylings HBM, Geyer S, Schäfer A, Turner R, Forstmann BU (2012) Are there
786 three subdivisions in the primate subthalamic nucleus? Front Neuroanat 6 Available
787 at: http://www.ncbi.nlm.nih.gov/pmc/articles/PMC3349268/ [Accessed January 28,
788 2016].

789 Kim H, Lim C-S, Kaang B-K (2016) Neuronal mechanisms and circuits underlying repetitive
790 behaviors in mouse models of autism spectrum disorder. Behav Brain Funct 12:3.

791 Kita H, Kitai ST (1987) Efferent projections of the subthalamic nucleus in the rat: light and
792 electron microscopic analysis with the PHA-L method. J Comp Neurol 260:435–452.

793 Kontis D, Theochari E (2012) Dopamine in anorexia nervosa: a systematic review. Behav
794 Pharmacol 23:496–515.

795 Lambert C, Zrinzo L, Nagy Z, Lutti A, Hariz M, Foltynie T, Draganski B, Ashburner J,
796 Frackowiak R (2015) Do we need to revise the tripartite subdivision hypothesis of the
797 human subthalamic nucleus (STN)? Response to Alkemade and Forstmann.
798 NeuroImage 110:1–2.

799 Lardeux S, Paleressompoulle D, Pernaud R, Cador M, Baunez C (2013) Different populations
800 of subthalamic neurons encode cocaine vs. sucrose reward and predict future error. J
801 Neurophysiol 110:1497–1510.

802 Lardeux S, Pernaud R, Paleressompoulle D, Baunez C (2009) Beyond the Reward Pathway:
803 Coding Reward Magnitude and Error in the Rat Subthalamic Nucleus. J Neurophysiol
804 102:2526–2537.

805 Liguz-Lecznar M, Skangiel-Kramska J (2007) Vesicular glutamate transporters (VGLUTs):
806 the three musketeers of glutamatergic system. Acta Neurobiol Exp (Warsz) 67:207–
807 218.

808 Ljungdahl A, Hanrieder J, Falth M, Bergquist J, Andersson M (2011) Imaging mass
809 spectrometry reveals elevated nigral levels of dynorphin neuropeptides in L-DOPA-
810 induced dyskinesia in rat model of Parkinson's disease. PLoS One 6:e25653.

811 Mahmoudi S, Levesque D, Blanchet PJ (2014) Upregulation of dopamine D3, not D2,
812 receptors correlates with tardive dyskinesia in a primate model. Mov Disord 29:1125–
813 1133.

814 Mallet L et al. (2008) Subthalamic Nucleus Stimulation in Severe Obsessive–Compulsive
815 Disorder. N Engl J Med 359:2121–2134.

816 Martin DM, Skidmore JM, Philips ST, Vieira C, Gage PJ, Condie BG, Raphael Y, Martinez
817 S, Camper SA (2004) PITX2 is required for normal development of neurons in the
818 mouse subthalamic nucleus and midbrain. Dev Biol 267:93–108.

819 Menegas W, Bergan JF, Ogawa SK, Isogai Y, Venkataraju KU, Osten P, Uchida N, Watabe-
820 Uchida M (2015) Dopamine neurons projecting to the posterior striatum form an
821 anatomically distinct subclass. eLife 4:e10032.

822 Moechars D, Weston MC, Leo S, Callaerts-Vegh Z, Goris I, Daneels G, Buist A, Cik M, van
823 der Spek P, Kass S, Meert T, D'Hooge R, Rosenmund C, Hampson RM (2006)
824 Vesicular glutamate transporter VGLUT2 expression levels control quantal size and
825 neuropathic pain. J Neurosci Off J Soc Neurosci 26:12055–12066.

826 Olanow CW, Tatton and WG (1999) Etiology and Pathogenesis of Parkinson's Disease.
827 Annu Rev Neurosci 22:123–144.

828 Orduna AR, Beaudry F (2016) Characterization of endoproteolytic processing of dynorphins
829 by proprotein convertases using mouse spinal cord S9 fractions and mass
830 spectrometry. Neuropeptides 57:85–94.

831 Parent A, Hazrati LN (1995) Functional anatomy of the basal ganglia. II. The place of
832 subthalamic nucleus and external pallidum in basal ganglia circuitry. Brain Res Brain
833 Res Rev 20:128–154.

834 Parent A, Sato F, Wu Y, Gauthier J, Lévesque M, Parent M (2000) Organization of the basal
835 ganglia: the importance of axonal collateralization. Trends Neurosci 23:S20–S27.

836 Pelloux Y, Baunez C (2013) Deep brain stimulation for addiction: why the subthalamic
837 nucleus should be favored. Curr Opin Neurobiol 23:713–720.

838 Pratt WE, Choi E, Guy EG (2012) An examination of the effects of subthalamic nucleus
839 inhibition or μ-opioid receptor stimulation on food-directed motivation in the non-
840 deprived rat. Behav Brain Res 230:365–373.

841 Pupe S, Schweizer N, Wallen-Mackenzie A (2015) Reply to Konsolaki and Skaliora:
842 Habituation, hyperlocomotion, and "genuine hyperlocomotion." Proc Natl Acad Sci U
843 A 112:E5.

844 Rico AJ, Barroso-Chinea P, Conte-Perales L, Roda E, Gómez-Bautista V, Gendive M, Obeso
845 JA, Lanciego JL (2010) A direct projection from the subthalamic nucleus to the
846 ventral thalamus in monkeys. Neurobiol Dis 39:381–392.

847 Rodriguez MC, Obeso JA, Olanow CW (1998) Subthalamic nucleus-mediated excitotoxicity
848 in parkinson's disease: A target for neuroprotection. Ann Neurol 44:S175–S188.

849 Rouaud T, Lardeux S, Panayotis N, Paleressompoulle D, Cador M, Baunez C (2010)
850 Reducing the desire for cocaine with subthalamic nucleus deep brain stimulation. Proc
851 Natl Acad Sci U S A 107:1196–1200.

852 Sanchis-Segura C, Spanagel R (2006) Behavioural assessment of drug reinforcement and
853 addictive features in rodents: an overview. Addict Biol 11:2–38.

854 Sato F, Parent M, Levesque M, Parent A (2000) Axonal branching pattern of neurons of the
855 subthalamic nucleus in primates. J Comp Neurol 424:142–152.

856 Schwartz JC, Diaz J, Bordet R, Griffon N, Perachon S, Pilon C, Ridray S, Sokoloff P (1998)
857 Functional implications of multiple dopamine receptor subtypes: the D1/D3 receptor
858 coexistence. Brain Res Brain Res Rev 26:236–242.

859 Schweizer N, Pupe S, Arvidsson E, Nordenankar K, Smith-Anttila CJA, Mahmoudi S,
860 Andrén A, Dumas S, Rajagopalan A, Lévesque D, Leão RN, Wallén-Mackenzie Å
861 (2014) Limiting glutamate transmission in a Vglut2-expressing subpopulation of the
862 subthalamic nucleus is sufficient to cause hyperlocomotion. Proc Natl Acad Sci U S A
863 111:7837–7842.

864 Shen K-Z, Johnson SW (2008) Complex EPSCs evoked in substantia nigra reticulata neurons
865 are disrupted by repetitive stimulation of the subthalamic nucleus. Synapse 62:237–
866 242.

867 Shen Y-C, Liao D-L, Lu C-L, Chen J-Y, Liou Y-J, Chen T-T, Chen C-H (2010)
868 Resequencing of the vesicular glutamate transporter 2 gene (VGLUT2) reveals some
869 rare genetic variants that may increase the genetic burden in schizophrenia. Schizophr
870 Res 121:179–186.

871 Shirayama Y, Chaki S (2006) Neurochemistry of the nucleus accumbens and its relevance to
872 depression and antidepressant action in rodents. Curr Neuropharmacol 4:277–291.

873 Skidmore JM, Cramer JD, Martin JF, Martin DM (2008) Cre fate mapping reveals lineage
874 specific defects in neuronal migration with loss of Pitx2 function in the developing
875 mouse hypothalamus and subthalamic nucleus. Mol Cell Neurosci 37:696–707.

876 Skinner BF (1966) The phylogeny and ontogeny of behavior. Contingencies of reinforcement
877 throw light on contingencies of survival in the evolution of behavior. Science
878 153:1205–1213.

879 Stice E, Spoor S, Bohon C, Small DM (2008) Relation between obesity and blunted striatal
880 response to food is moderated by TaqIA A1 allele. Science 322:449–452.

881 Takamori S (2006) VGLUTs: "Exciting" times for glutamatergic research? Neurosci Res
882 55:343–351.

883 Temel Y, Blokland A, Steinbusch HWM, Visser-Vandewalle V (2005a) The functional role
884 of the subthalamic nucleus in cognitive and limbic circuits. Prog Neurobiol 76:393–
885 413.

886 Temel Y, Visser-Vandewalle V, Aendekerk B, Rutten B, Tan S, Scholtissen B, Schmitz C,
887 Blokland A, Steinbusch HW (2005b) Acute and separate modulation of motor and
888 cognitive performance in parkinsonian rats by bilateral stimulation of the subthalamic
889 nucleus. Exp Neurol 193:43–52.

890 Uslaner JM, Dell'Orco JM, Pevzner A, Robinson TE (2007) The Influence of Subthalamic
891 Nucleus Lesions on Sign-Tracking to Stimuli Paired with Food and Drug Rewards:
892 Facilitation of Incentive Salience Attribution? Neuropsychopharmacology 33:2352–
893 2361.

894 Val-Laillet D, Aarts E, Weber B, Ferrari M, Quaresima V, Stoeckel LE, Alonso-Alonso M,
895 Audette M, Malbert CH, Stice E (2015) Neuroimaging and neuromodulation
896 approaches to study eating behavior and prevent and treat eating disorders and obesity.
897 NeuroImage Clin 8:1–31.

898 Volkow ND, Fowler JS, Wang GJ, Baler R, Telang F (2009) Imaging dopamine's role in drug
899 abuse and addiction. Neuropharmacology 56 Suppl 1:3–8.

900 Volkow ND, Wang GJ, Fowler JS, Logan J, Gatley SJ, Gifford A, Hitzemann R, Ding YS,
901 Pappas N (1999) Prediction of reinforcing responses to psychostimulants in humans
902 by brain dopamine D2 receptor levels. Am J Psychiatry 156:1440–1443.

903 Waddington JL, Clifford JJ, McNamara FN, Tomiyama K, Koshikawa N, Croke DT (2001)
904 The psychopharmacology-molecular biology interface: exploring the behavioural roles
905 of dopamine receptor subtypes using targeted gene deletion ('knockout'). Prog
906 Neuropsychopharmacol Biol Psychiatry 25:925–964.

907 Wallén-Mackenzie A, Gezelius H, Thoby-Brisson M, Nygård A, Enjin A, Fujiyama F, Fortin
908 G, Kullander K (2006) Vesicular glutamate transporter 2 is required for central
909 respiratory rhythm generation but not for locomotor central pattern generation. J
910 Neurosci Off J Soc Neurosci 26:12294–12307.

911 Wang GJ, Volkow ND, Logan J, Pappas NR, Wong CT, Zhu W, Netusil N, Fowler JS (2001)
912 Brain dopamine and obesity. Lancet 357:354–357.

913 Watabe-Uchida M, Zhu L, Ogawa SK, Vamanrao A, Uchida N (2012) Whole-Brain Mapping
914 of Direct Inputs to Midbrain Dopamine Neurons. Neuron 74:858–873.

915 Wenzel JM, Cheer JF (2014) Endocannabinoid-dependent modulation of phasic dopamine
916 signaling encodes external and internal reward-predictive cues. Front Psychiatry
917 5:118.

918 Williams A, Gill S, Varma T, Jenkinson C, Quinn N, Mitchell R, Scott R, Ives N, Rick C,
919 Daniels J, Patel S, Wheatley K, Group PSC (2010) Deep brain stimulation plus best
920 medical therapy versus best medical therapy alone for advanced Parkinson's disease
921 (PD SURG trial): a randomised, open-label trial. Lancet Neurol 9:581–591.

922 Yakovleva T, Bazov I, Cebers G, Marinova Z, Hara Y, Ahmed A, Vlaskovska M, Johansson
923 B, Hochgeschwender U, Singh IN, Bruce-Keller AJ, Hurd YL, Kaneko T, Terenius L,
924 Ekström TJ, Hauser KF, Pickel VM, Bakalkin G (2006) Prodynorphin storage and
925 processing in axon terminals and dendrites. FASEB J Off Publ Fed Am Soc Exp Biol
926 20:2124–2126.

## Figure Legends

**Figure 1: Strong overlap of Vglut2 and Pitx2 in the STN and reduction of Vglut2 mRNA in cKO mice.**

**A:** Representative examples of cell morphology and distribution. Overview of the STN (left) as well as close-up images of the dorsal (right top), ventral (right center) and medial (right bottom); cells are stained blue, small dots represent silver grains bound to Vglut2 mRNA. **B:** double fluorescent *in situ* hybridization for Vglut2 (red) and Pitx2 (green) as well as nuclear stain with DAPI (blue) in the dorsal (top), ventral (center) and medial (bottom) STN. **C:** High resolution *in situ* hybridization analysis of Vglut2 mRNA-based silver grain intensity showed a generally lowered expression of Vglut2 in the STN of cKO mice.

cKO: conditional knock-out; STN: subthalamic nucleus.

**Figure 2: Decreased consumption of sugar in STN-VGLUT2 cKO mice.**

**A:** Schematic self-administration (SA) schedule. Black lines indicate the number of days during which each paradigm was carried out. **B:** Operant SA was carried out in modular SA boxes with two feeders, of which one was delivering pellets upon head entry (south, green = active), while the other was not (north, red = inactive). Yellow: house light, black bars: head entry holes measuring exploration with no feeder attached. When a mouse made a head entry at the active feeder, a sugar reward was delivered, and simultaneously, a light and a sound cue were presented to confirm the choice (left), while a head entry at the inactive feeder produced neither reward delivery, nor a light or sound cue (right). **C:** During task learning, both Ctrls (white circles) and cKOs (filled circles) decreased time to obtain the maximum of 30 sugar pellets. **D:** During FR1, the time to consume 30 pellets was significantly higher for cKOs (filled circles) compared to Ctrls (white circles) (left panel). All mice were able to obtain the maximum of 30 pellets during the FR1 protocol (middle panel). The amount of head entries during the inactive time (timeout) decreased in cKOs, while Ctrls increased (right). **E:** During

FR5, head entries during active time (left), the amount of pellets obtained (middle) and head entries during inactive time (right) were lower for cKOs compared to Ctrls. **F:** During progressive ratio (PR), no difference was seen in head entries during the active (left) or the inactive time (timeout, right) between Ctrls and cKO mice. **G:** Cognitive ability testing. During reinstatement, the mice were presented to the original task after an extinction period (left). During reversal, the positions of the active and inactive feeders were switched (right). **H:** To allow testing of the retention of the task (reinstatement), both cKO and Ctrl groups were put through extinction. For 5 consecutive days, the active feeder delivered both light and sound cues, but no sugar pellets. For both groups, the amount of head entries strongly decreased during both the active time (left) and during timeout (right). **I:** No differences between Ctrl and cKO mice were seen during reinstatement or reversal.

Statistical analysis of the SA data was performed using repeated-measures ANOVA followed by a post-hoc test with Bonferroni correction. #/* $p \leq 0.05$; ##/** $p \leq 0.01$; ###/*** $p \leq 0.001$, ####/**** $p \leq 0.0001$. cKO: conditional knock-out; Ctrl: control; d: day; Extinct. Extinction; FR: fixed ratio; Hab.: habituation; minutes: minutes; PR: progressive ratio; Rev.: reversal; RI: reinstatement; s: seconds.

**Figure 3: The average weight of STN-VGLUT2 cKO mice is decreased, while home cage food consumption is unaltered.**

**A:** Ctrl mice (white circles) had a higher body weight than cKO (filled circles) over the course of the experiment. **B:** Refeeding after SA was not significantly different between Ctrls and cKOs.

Statistical analysis of weight and food intake data were analyzed using repeated measures ANOVA followed by a post-hoc test with Bonferroni correction. * $p \leq 0.05$; ** $p \leq 0.001$. cKO: conditional knock-out; Ctrl: control; g: gram; h: hours; SA: self-administration.

**Figure 4: Increased seated and free rearing in STN-VGLUT2 cKO mice.**

Three different rearing types were observed in STN-VGLUT2 cKO mice: wall rearing, where the mouse takes support against a vertical surface (A, left),; seated rearing, where the mouse supports itself on the tail base (B, left),, and free rearing, where the mouse stretches its hind legs and uses no other support (C, left),. All rearing types were scored in an open field arena. Both groups were habituated to the environment (# marks the change over time), cKOs show increased seated (B) and free (C) rearing throughout the session (¤ marks the difference between genotypes and * marks the difference at a certain time point between genotypes). Rearing data was analyzed by repeated measures ANOVA and post-hoc test with Bonferroni correction. * $p \leq 0.05$; ** $p \leq 0.001$; *** $p \leq 0.0001$. cKO: conditional knock-out; Ctrl: control.

**Figure 5: The availability of dopamine receptor D2 and D3 as well as DAT binding sites in the ventral striatum is regulated by Vglut2 reduction in the STN.**

**A:** Representative examples of serial coronal striatal sections analyzed for DAT, D1R, D2R and D3R (from top to bottom). **B:** Comparison of specific binding capacity levels expressed as percent of control for DAT-specific [125I] RTI binding, D1R-specific [3H] SCH23390, D2R-specific [125I] Iodosulpride and D3R-specific [125I]-7-OH-PIPAT binding in Ctrl and cKO mice. DAT binding was unaltered in the NAcC and upregulated in the NAcSh of cKO mice (left). The amount of D1 receptor binding sites (middle left) in both NAcC and NAcSh remained unaltered, whereas more D2 receptor binding sites were measured in both NAcC and NAcSh (middle right) and less D3 receptor binding sites were available in NAcSh (right). Data analyzed by Mann-Whitney U-test. * $p \leq 0.05$. cKO: conditional knock-out; Ctrl: control; NacC, nucleus accumbens core; NAcSh: nucleus accumbens shell; STN: subthalamic nucleus.

**Figure 6: Elevated levels of dynorphin peptides in the NAc of STN-VGLUT2 cKO mice.**

**A:** MALDI analysis was performed on cryosections at the level of the DStr and NAc. Each slice was coated with droplets of matrix for ionization of the peptide fragments and analyzed

in MALDI-TOF. **B:** A brightfield (BF) picture of the cresyl violet-stained section analyzed for aNeo was used to determine the localization of DStr and NAc (black outlines). Representative examples of aNeo (depicted in red) in cKO. Overlays with peptide fragment m/z 1835 and m/z 1393 (middle and right, depicted in green) visualized the fiber bundles used as landmarks for the anatomical localization of the NAc. **C:** Representative examples of slices used for MALDI imaging in controls (left) and cKOs (right). aNeo and DynA peptide levels were significantly elevated in cKOs and showed a more restricted localization to the NAc. **D:** Fluorescence intensity of different peptides measured by MALDI imaging, shown as percent of control (fold change, see table). **E:** Example peaks of DynA (top) and aNeo (bottom) from MALDI analysis. **F:** Oligo in situ hybridization analysis of Dyn expression in the forebrain of Ctrl (left) and cKO (right) mice.

cKO: conditional knock-out. aNeo: alpha-neo-endorphin; cKO: conditional knock-out; Ctrl: control; DynA: dynorphin A; DynB: dynorphin B; FC: fold change; m/z: mass to charge ratio; numbers in brackets indicate, which amino acids constitute each peptide fragment. * $p \leq 0.05$ and ** $p \leq 0.01$; error given as S.E.M.

**Figure 7: Optogenetic tracing of Vglut2-Pitx2 co-expressing neurons revealed a projection pattern restricted to the EP and SNr. A-C: Schematic illustrations of injection procedure. A:** Mice were stereotactically injected with AAV-ChR2-EYFP virus into the STN; **B:** The injection was performed bilaterally but one side at a time to infect the left- and right-hand side STN at equal levels; **C:** Two close coordinates were used for each STN to allow even spread of the virus (-4.25 and -4.75 DV). D: Histological results of injections. AAV-ChR2-EYFP-positive cell bodies in the STN. E: AAV-ChR2-EYFP-positive fibers projecting to EP (left), GP (middle) and SNr (right). Upper row: EYFP expression. Lower row: bright field photographs of the same area.

EP: entopeduncular nucleus; GP: globus pallidus; SNr: substantia nigra pars reticulata; PSTN: parasubthalamic nucleus; STN: subthalamic nucleus.

**Figure 8: Vglut2 reduction leads to cell loss and reduction in size of STN.**

**A:** Cell size is increased in cKO (black bars) mice compared to Ctrls (white bars). The cKOs show a much wider spread of cell size than Ctrls **B:** Representative pictures of STN morphology in cKOs and Ctrls. The STN of cKO mice appears slimmer compared to controls. The white outlines were used for 2D and 3D analysis of STN morphology. **C:** 2D analysis of STN morphology. The size of the STN was assessed by measuring the diameter of the STN at its widest point and comparing it to the diameter of the cp and the total diameter of both structures at the same point. **D:** Representative example of a Ctrl (left, red) and a cKO STN (middle, green), and their overlay (right). Both diameter (white dotted line) and volume of the cKO STN is reduced compared to the Ctrl.

3D reconstruction was obtained with MATLAB from 16 and 27 images of a cKO and a Ctrl, respectively. cKO: conditional knock-out; cp: cerebral peduncle; Ctrl: control; STN: subthalamic nucleus.

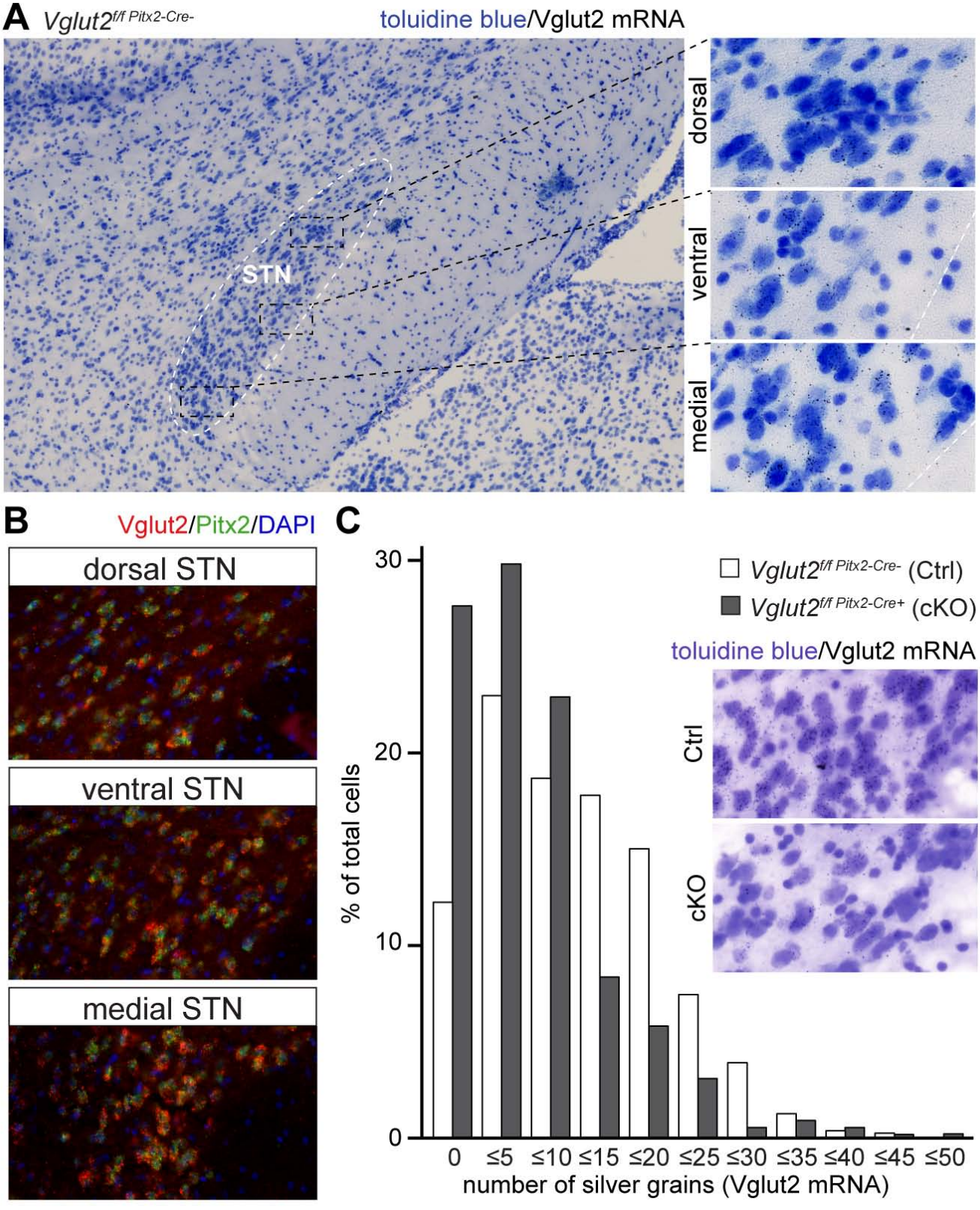

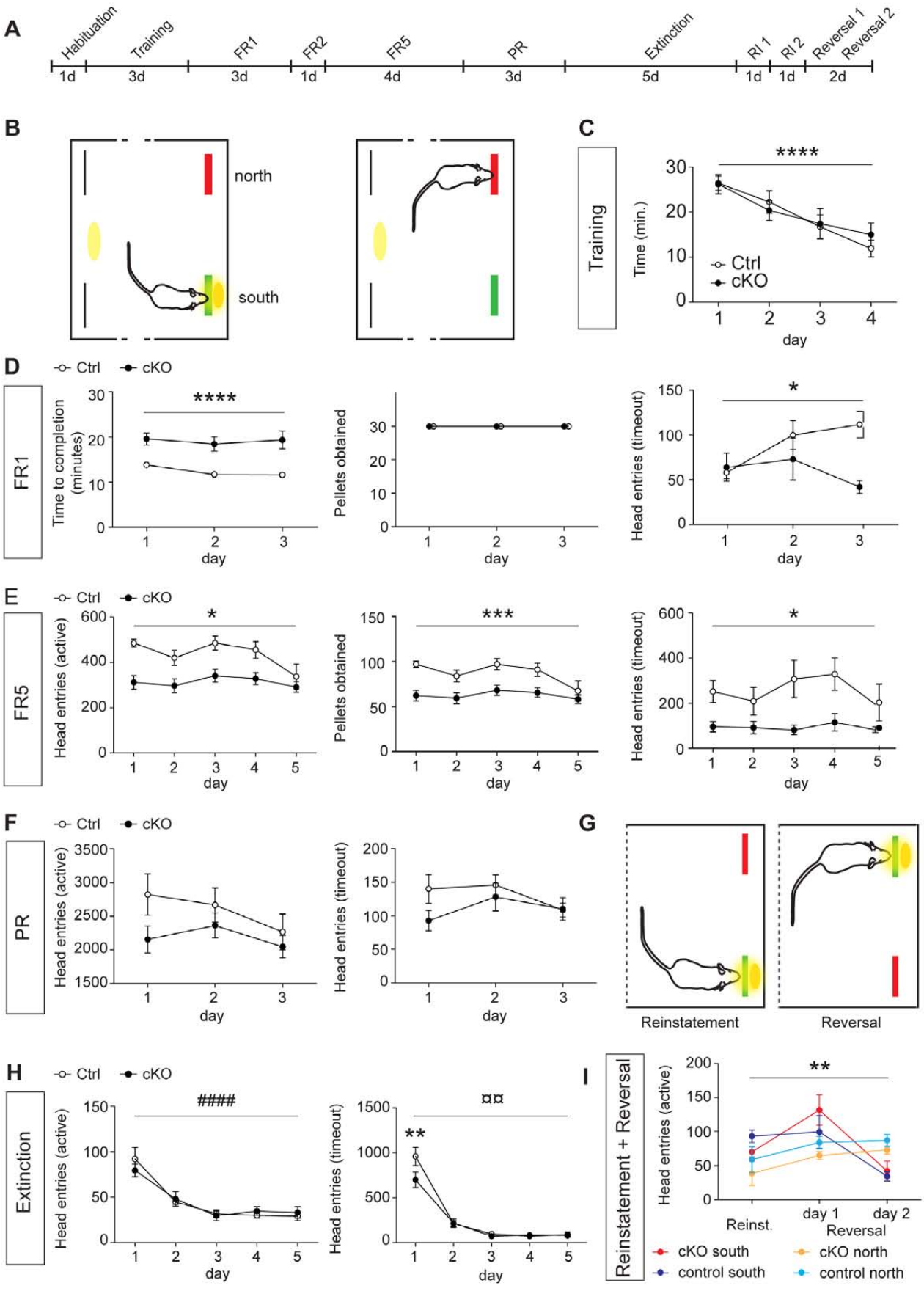

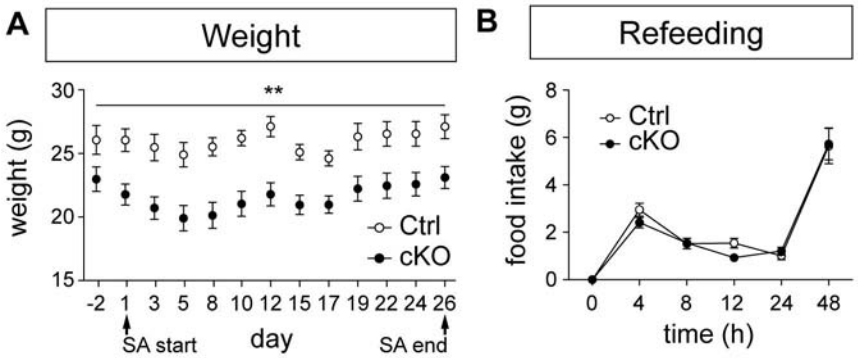

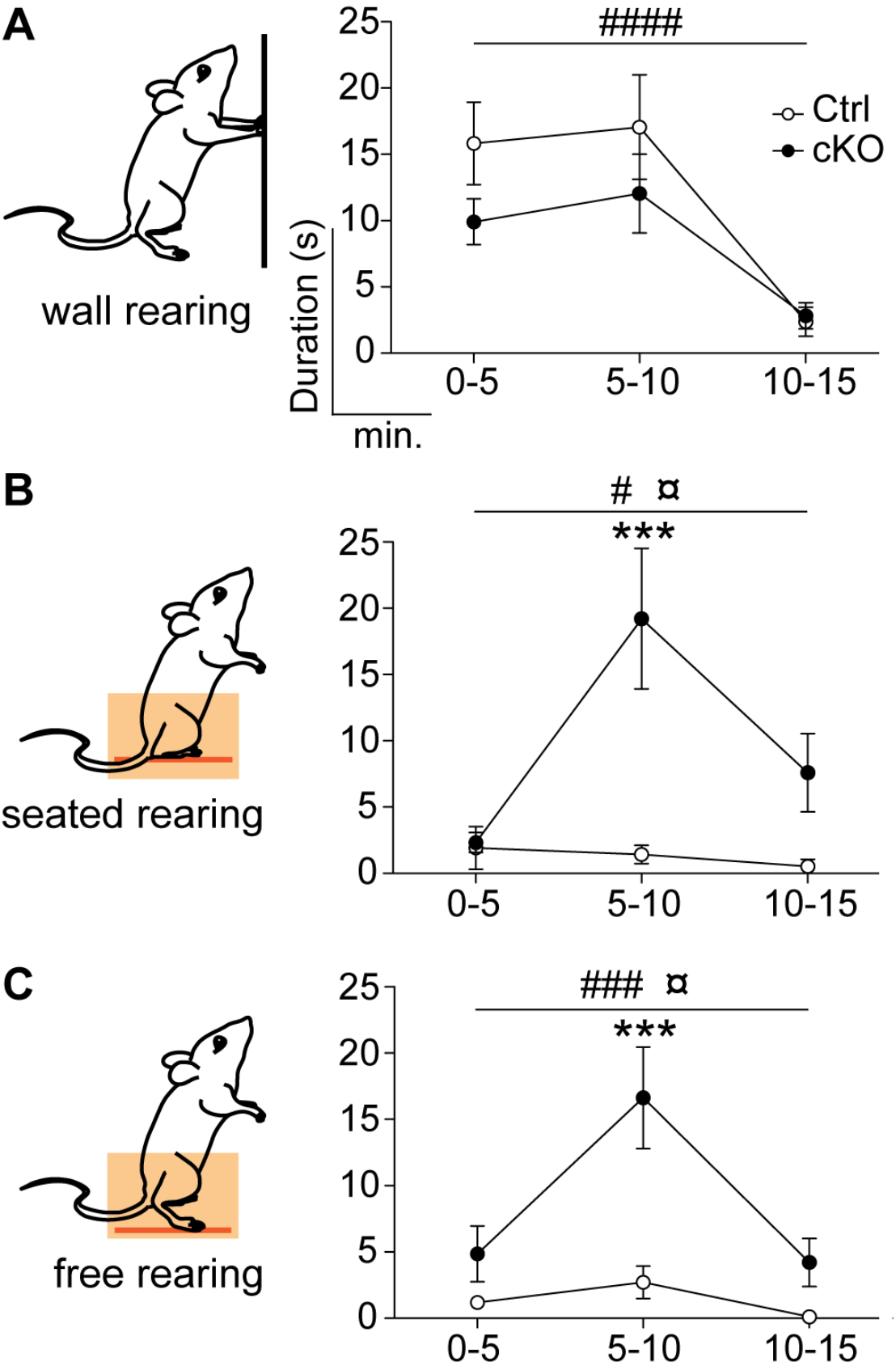

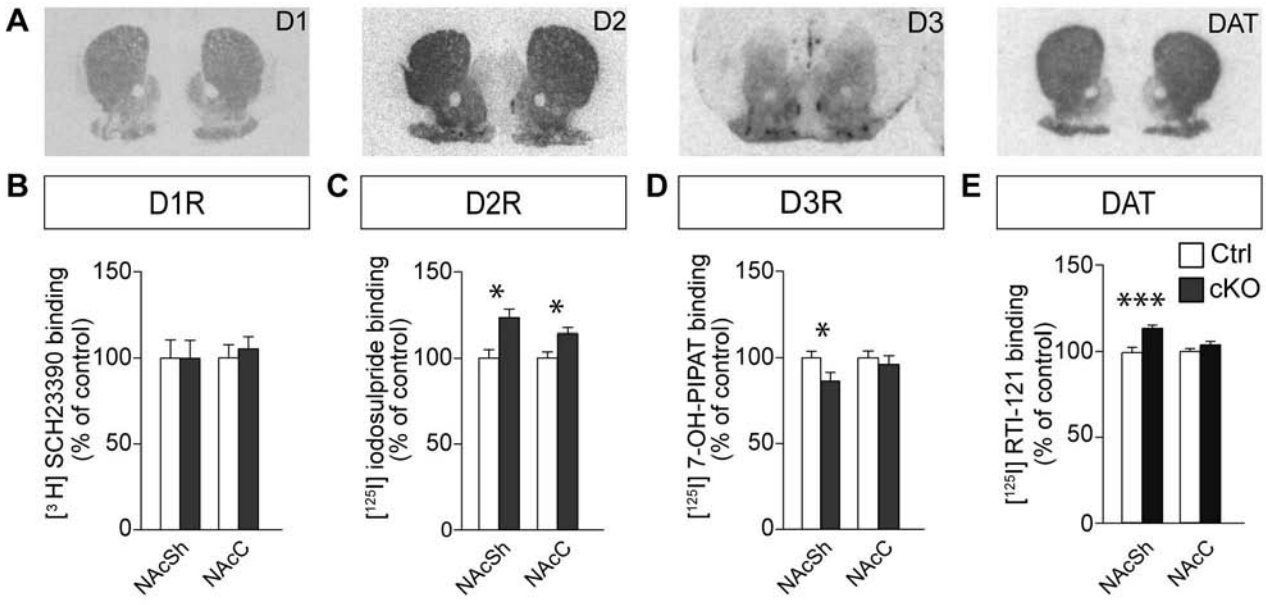

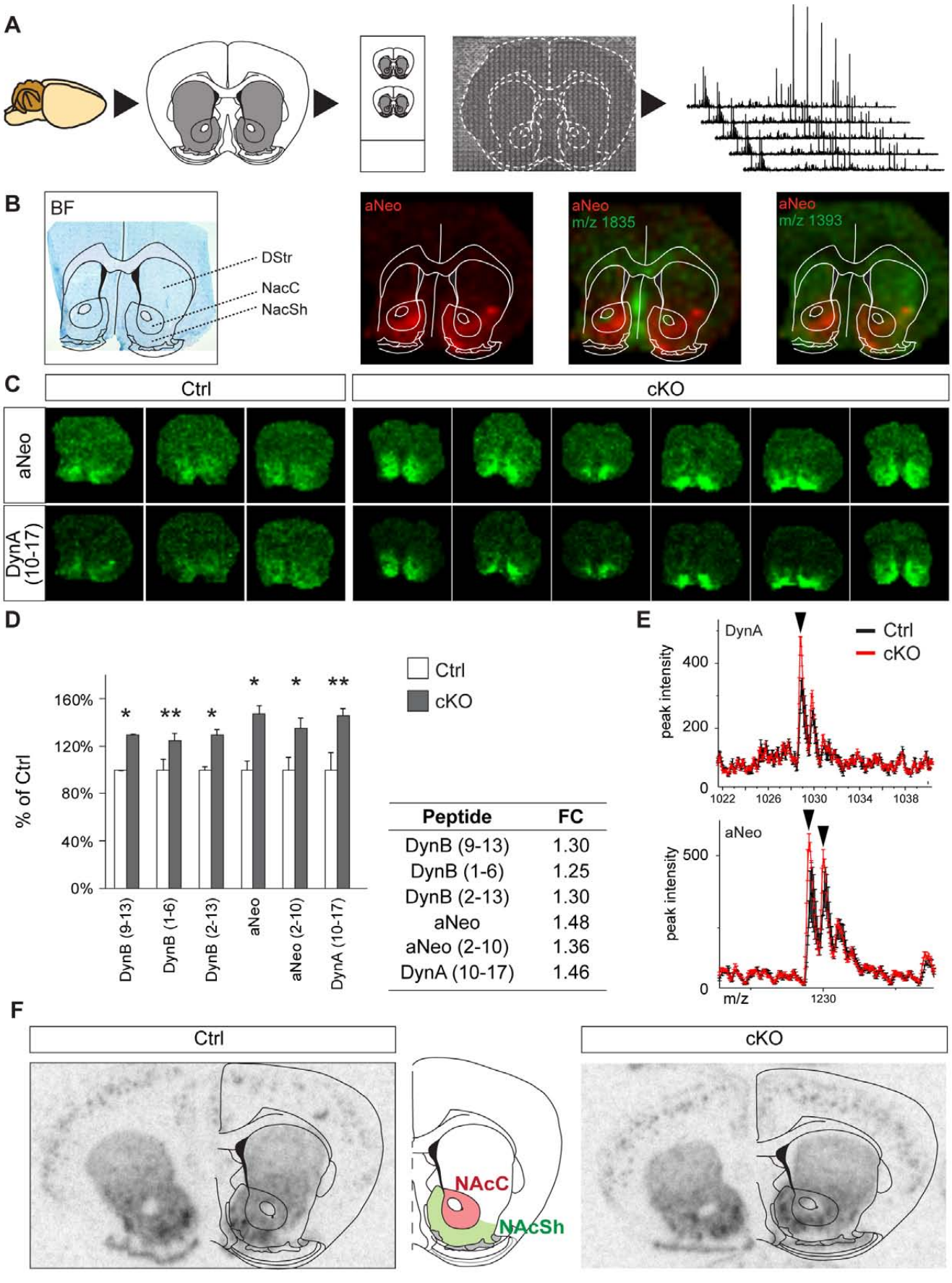


| Peptide | FC |
|---|---|
| DynB (9-13) | 1.30 |
| DynB (1-6) | 1.25 |
| DynB (2-13) | 1.30 |
| aNeo | 1.48 |
| aNeo (2-10) | 1.36 |
| DynA (10-17) | 1.46 |